An Efficient approach for Undelayed Range-only SLAM based on Gaussian Mixtures Expectation☆

Felipe R. Fabresse, Fernando Caballero, Iván Maza and Aníbal Ollero

University of Seville, Escuela Técnica Superior de Ingeniería
Camino de los Descubrimientos s/n, 41092 Sevilla (Spain)
`fabresse@us.es, fcaballero@us.es, imaza@us.es, aollero@us.es`

Abstract

This paper deals with range-only simultaneous localization and mapping (RO-SLAM), which is of particular interest in aerial robotics where low-weight range-only devices can provide a complementary continuous estimation between robot and landmarks when using radio-based sensors. Range-only sensors work at greater distances when compared to other commonly used sensors in aerial robotics and they are low-cost. However, the spherical shell uniform distribution inherent to range-only observations poses significant technological challenges, restricting the approaches that can be used to solve this problem. This paper presents an undelayed multi-hypothesis Extended Kalman Filter (EKF) approach based on Gaussian Mixture Models (GMM) and a reduced parameterization of the state vector to improve its efficiency. The paper also proposes a new robot-to-landmark and landmark-to-landmark range-only observation model for EKF-SLAM which takes advantage of the reduced parameterization. Finally, a new scheme is proposed for updating hypothesis weights based on an independence of beacon parameters. The method is firstly validated with simulations comparing the results with other state-of-the-art methods and later validated with real experiments for 3D RO-SLAM using several radio-based range-only sensors and an aerial robot.

Keywords: range-only simultaneous localization and mapping, robot localization, Kalman filtering, Gaussian Mixture Models.

1. Introduction

Range-only simultaneous localization and mapping (RO-SLAM) aims to map the position of a set of elements (landmarks) while at the same time localizing a mobile robot with respect to that map using range-only observations. In contrast to other SLAM approaches, the main challenge of RO-SLAM is the
5 rank-deficiency of the range-only observation model. These observations consist of a single value which represents the distance between a pair of elements (robot or landmarks). Thus, given a single range-only observation, the lack of bearing information between these two elements makes the relative position between them follow a uniform spherical shell probability distribution as is shown in Fig. 1 for a single range-only observation between an aerial robot and a landmark. Furthermore, in contrast to other schemes like bearing-
10 only SLAM [1], RO-SLAM presents an increased complexity for higher dimensionality (e.g. 3D SLAM in aerial robotics) due to the 1-rank observation model associated with range-only observations (azimuth and elevation angle not observed) compared to other bearing-only models in which the only unobserved parameter is the distance between the robot and one landmark, or other fully observable approaches like RFID SLAM[2, 3]. Hence, when applying multi-hypothesis approaches, this rank-deficiency implies a higher
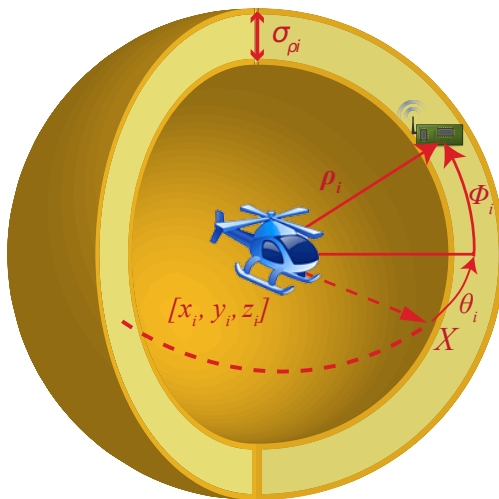15 number of hypotheses/parameters in the state vector.

Figure 1: Spherical parameterization of a landmark position in 3D RO-SLAM. The yellow area represents the uniform spherical shell distribution where the landmark might be located with a single range-only observation ρ_i between an aerial robot and this landmark. The green object represents the real position of the landmark, whereas the center of the sphere is composed by the position of the aerial robot at the time the range-only observation is received. The thickness of the 3D shell represents the standard deviation of the range measurement σ_{ρ_i}.

Range-only methods have gained research interest in the last decade particularly for robot/people/object indoor localization and ubiquitous applications among others and more recently in aerial robotics for radio frequency source localization in military, rescue, aerial manipulation or inspection scenarios. RO-SLAM becomes especially interesting in aerial robotics due to the small size and low weight associated to these kind of sensors. Additionally, most range-only sensors include a unique identifier in their signal that simplifies the common data association problem present in other SLAM schemes. RO-SLAM algorithms becomes a good complement to other SLAM approaches where a direct line of sight between robot and landmark is not always possible due to high altitudes or static/dynamic obstacles as is the case for cameras or LIDAR sensors [4].

Depending on the kind of technology employed to measure the distance between a pair of sensors (e.g. radio-based or ultrasound range-only sensors), different ranging methodologies are proposed in the literature: the most common is based on the radio signal strength of ranging messages [5, 6] (also known as Radio Signal Strength Indicator or RSSI range-only sensors), or the time of arrival (TOA) or Time Differential of Arrival (TDOA) of the signal [7, 8, 9] for radio and/or ultrasound range-only sensors.

The main research interest of range-only methods resides in how to cope with the spherical shell uniform distribution of the position as shown in Fig. 1. Thus, in the case of range-only localization several methods [10, 11, 12] are based on numerical optimization approaches which trilaterates the position of the mobile robot employing 3 or more static ranging nodes (also known as anchors) at different positions. On the other hand, [13] proposes a fingerprinting method using a neural network which is particularly useful when RSSI-based devices are used. Fuzzy logic has also been used for range-only localization [12] employing a Voronoi diagram to cope with common flip ambiguities in the probability distribution associated to range-only estimations. Other range-only localization approaches are based on Bayesian filters [10, 14, 15] or batch-processing techniques [16].

In the case of mapping problems, the estimated variables are the position of a set of static elements or landmarks (also known as self-localization or network localization). Three common approaches are used for mapping: one based on the use of inter-node range-only observations to estimate the relative position of static nodes, another based on the use of mobile robots with known position to trilaterate the position of each individual landmark using non-linear optimization methods and finally, a hybrid approach which combines the advantages of both methods. Some early works use batch-processing techniques like Multidimensional

Scaling (MDS) [17] or Least square methods [18] to map the relative position of each node. However MDS methods require a high connectivity between static nodes to localize each of them, which is why other authors proposed different approaches based on sub-map estimation [19] or the use of artificial nodes created from a set of range measurements taken from different robot positions [20]. Other authors have used decentralized inference to solve the mapping problem by means of multilateration from a mobile robot usign probablistic frameworks like particle filters [21, 22]. Particle filters model the inherent spherical shell uniform distribution of range-only landmarks position by using Monte Carlo sampling methods.

In the case of Gaussian filters, authors tend to use two common approaches: the first and most common consists on a delayed initialization of the Gaussian filter based on a pre-estimated position of landmarks [23, 21, 24] and the second approach uses undelayed initialization based on multi-hypotheses frameworks to cope with the non-Gaussian distribution of landmark positions. However, in delayed initialization approaches, single estimation convergence will always depend on the robot's trilateration with respect the landmark so that important delays might be produced until these landmarks converge and can be integrated in the Gaussian filter used to refine the robot position. On the other hand, undelayed approaches have the advantage of integrating range-only observations into the Gaussian filter since the very beginning without loss of information and, more importantly, they are able to improve the robot's position estimation without requiring single solution convergence of landmarks. One of these undelayed approaches [25] is based on a polar parameterization which allows the Gaussian filter to be initialized using a predefined variance around the $\rho\theta$-space. The main drawback of this approach is the use of heuristics based on the robot trajectory to split the initial unimodal distribution into two Gaussians which, in the case of 3D RO-SLAM, becomes more complex. In [26] a method is proposed which integrates a Gaussian Mixture in an Extended Kalman Filter (EKF) to represent the non-Gaussian distribution of the sensor's bearing information. This approach has the additional advantage of making the integration of inter-node range-only observations without losing cross correlation information between landmarks possible as is the case of the decentralized approach presented in [25]. The main drawback of multi-hypothesis methods is the computational burden of keeping all possible hypotheses in the system. To cope with this drawback, [26] uses a pruning strategy which allows the computational burden of the multi-hypothesis approach to be reduced as landmarks converge to a single solution. In a previous work, the authors of this article proposed an extended version of [26] which deals with higher dimensionalities by using a reduced parameterization approach. The method proposed in this paper extends the 3D approach presented in [27] by introducing a new observation model for range-only measurements which only requires a single update equation as opposed to the Federated Information Sharing approach [1] inherited from [26]. The paper compares the computational burden and accuracy obtained with the new correction model with respect to previous observation models based on Federated Information Sharing. Also, this paper shows a scheme for updating Gaussian Mixture weights based on the same independence assumption between beacon parameters proposed in [27]. This paper will show both how the reduced parameterization and how the new range-only observation model might be used with other approaches (i.e. for example, how new observation model might be used with a Cartesian parametrization, or how the reduced parameterization might be used with other classical range-only observation models). The use of the reduced parameterization proposed in [27] does not imply an independence between beacon parameters, so other classical approaches might be used to update the weights of the Gaussian Mixtures.

For the case of range-only simultaneous localization and mapping, different frameworks have been proposed in the literature. Some authors employ batch-processing methods like [28, 29] which solves the problem as an optimization problem. Even though batch-processing methods present accurate results, they are not suitable for online estimation. Other authors use probabilistic frameworks which are suitable for online estimation and can model most belief distributions present in robotic applications [30]. A comparison of most common SLAM frameworks is done in [31, 32], where the Unscented FastSLAM presents better performance results over other classical approaches like EKF-SLAM or UKF-SLAM. FastSLAM is based on the factorization of the map using a Rao-blackwellization of the robot and map probability distribution, allowing the estimation of individual landmarks position and the robot position to be separated. Instead of using a Gaussian filter, FastSLAM factorizes the map by using a Monte Carlo sampling approach to model the relation between the localization and map belief, thus having a different map probability distribution per localization sample.
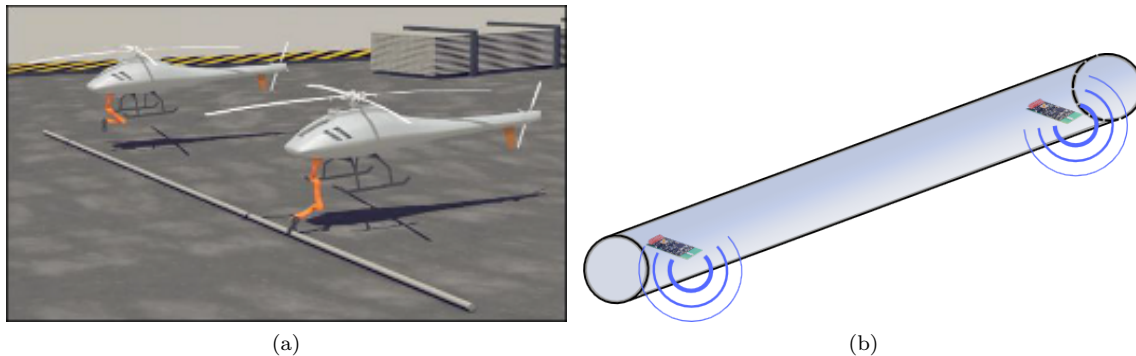
<center>(a)   (b)</center>

Figure 2: ARCAS project: Aerial Robotics Cooperative Assembly System (`http://arcas-project.eu`). (a) aerial robots endowed with manipulators grasping a bar and (b) bars with two embedded radio range-only sensors at the ends of bars so that robots endowed with manipulators can estimate the pose of these bars.

Some solutions based on the FastSLAM framework use optimized particle filters not only to estimate the position of the robot but also for landmarks position. These particle filters are optimized by means of a reduction in the number of particles [33] or by using an adaptive resampling method [34]. FastSLAM is typically implemented with EKFs for map estimation since it improves the efficiency of landmark estimation using both delayed [35, 36] and undelayed strategies [37]. However, when the system includes high correlation constraints between landmarks, as is the case for those applications which includes range-only measurements between landmarks, Rao-blackwellization can no longer be applied to factorize the map. As an example, in the ARCAS project (`http://arcas-project.eu`) shown in Fig. 2, some radio-based range-only sensors are embedded into structure parts so that they can be localized by different robots endowed with manipulators whose mission is to assemble a structure cooperatively. In this application, strong correlations are introduced in the filter by using range-only observations between landmarks and integrating with a very low deviation the known constraints in the relative position of landmarks embedded in the same structure part.

Some approaches have already included range-only observations between landmarks in their RO-SLAM formulation [38, 25, 20] but without exploding the cross-correlation information of these landmarks. These range-only observations not only increase the speed of convergence of landmarks' hypothesis but also improve the mapping accuracy. This redundant information of inter-landmarks distance increases both reliability and precision of the map as demonstrated in [39] for multi-sensor fusion in SLAM and, indirectly, the localization of the robot through its correlation with landmarks. For this reason, range-only observations between landmarks might become especially informative in a centralized framework [27, 26, 25] like EKF-SLAM. In previous work of the authors of this article [27], 2D RO-SLAM was extended to 3D RO-SLAM by using the approach described in [26] in order to keep the correlation between landmarks. To the best of the authors' knowledge, there is no other implementation of centralized EKF for 3D RO-SLAM which takes advantage of correlations between landmarks. For this reason, in this paper the classical Federated Information Sharing approach has been implemented [1, 26] using three different parameterizations for comparison purpose. This paper extends the authors' previous work by including a new observation model for inter-landmark range-only measurements and shows how these measurements not only improves the speed of convergence and accuracy of the map but also improves the robot localization results.

This article is an improved and extended version of authors previous work [27] with the following main contributions:

1. an improved update scheme used to compute the new weights of Gaussian Mixtures. This allows to update one GMM weight taking into account other dependent GMM instead of just taking into account the most probable one.

2. a novel observation model used with range-only observations which only requires a single equation. This allows a huge reduction on the computational burden of the EKF correction stage per range-only observation and avoids having to split each observation variance as opposed to Federated Information

<center>4</center>

Sharing approaches since the observation is not duplicated for each hypotheses.

3. a new approach to integrate inter-node range-only observations (i.e. range-only observations between static range-only sensors) even when the filter has not yet converged to a single solution. This allows a faster convergence of filter hypothesis (reducing computational burden of the filter at earlier stages), a higher relative mapping accuracy and an indirect reduced robot localization error.

4. extended validation with more comparisons and more simulated and real experiments including multiple beacons (range sensors to be mapped), anchors (range sensors with known position) and an aerial robot.

The rest of the paper is organized as follows. A brief overview and comparison of different parameterizations with respect to the proposed reduced parameterization is presented in Sect. 2. A detailed description of the method is given in Sect. 3. Simulation and real experiments with multiple radio-based range sensors and an aerial robot are presented in Sect. 4. Finally, the paper is closed with some conclusions and future work in Sect. 5.

2. RO-SLAM parameterization in a nutshell

This section compares the reduced parameterization proposed in [27] with other RO-SLAM parameterizations used in the literature for multi-hypotheses approaches. Two important aspects should be taken into account when comparing the parameterizations used for an EKF-SLAM approach: first, the computational complexity of the Gaussian filters, which in the case of EKF, is highly dependent on the number of parameters of the state vector [30], and second, the scalability of the system with the number of landmarks.

The most common parameterization used in the literature for landmarks position is the Cartesian parameterization [37, 24]. In this parameterization, each hypotheses j of a landmark i is composed by Cartesian coordinates so that the total number of parameters for H hypotheses would be $2H$ ($f_{ij} = [x_{ij}, y_{ij}]^T$) for 2D and $3H$ ($f_{ij} = [x_{ij}, y_{ij}, z_{ij}]^T$) for 3D.

On the other hand, [40] proposed a polar parametrization for 2D RO-SLAM where each landmark position is parametrized as $f_i = [x_i, y_i, \rho_i, \theta_i]$. Here, x_i and y_i are the center of the annulus distribution from which the first range-only observation is received with a radius of ρ_i meters and the angle θ_i between the reference frame of the robot and landmark i. This polar parameterization fits better with 2D RO-SLAM since it allows the annular distribution of a single range-only observation to be represented using an elongated Gaussian in polar coordinates ($\rho\theta$-space). However, to represent the flip ambiguity which appears with the second range-only observation, the authors use a heuristic method to split the unimodal distribution into two Gaussian distributions as a result of the intersection between the first annulus distribution and the second generated with a new range-only observation. Thus, to represent these 2 hypotheses, polar parameterization uses 8 parameters (4 for each hypotheses) compared to 4 parameters needed in Cartesian parameterization for the same number of hypotheses. The main drawbacks of this parameterization are that it duplicates the common parameters x_i, y_i and ρ_i in both hypotheses and requires to delay the initialization of both hypotheses until a good trilateration is achieved to split the initial Gaussian distribution into two Gaussians. This is especially difficult in the case of 3D RO-SLAM where ambiguities are made worse. When inter-node range-only observations are integrated [25], this polar parametrization requires up to 5×2^m parameters to represent the initial spherical shell uniform distribution with m being the number of landmarks. In addition, as [25] is based on a decentralized solution, so it does not take into account the correlations between landmarks.

An extension of this polar parameterization was proposed in [26] for 2D RO-SLAM, in this case the authors use a Gaussian Mixture Model (GMM) to model the annular distribution of the landmark position belief. GMMs are probability distributions that are convex combination of Gaussian distributions, they form a semi-parametric alternative to non-parametric distributions, providing a better flexibility and precision when modeling the underlying statistics of range-only observations. In a GMM each mode i is a normal distribution $\mathcal{N}(\mu_i, \sigma_i)$ weighted by ω_i, where $0 \leq \omega_i \leq 1$ and $\sum_{i=1}^{k} \omega_i = 1$. Then, to represent the position hypothesis of a landmark i azimuth angle θ_i with N modes, the probability mass function $f_{\theta_i}(x)$ will look

like:

$$f_{\theta_i}(x) = \sum_{j=1}^{N} \omega_{\theta_{ij}} \mathcal{N}(x; \theta_{ij}, \sigma_{\theta_{ij}}) \tag{1}$$

With this parameterization, each landmark state is parameterized as $f_i = [x_i, y_i, \rho_i, \theta_{i1}, ..., \theta_{iN}]^T$. Thus, when the number of hypotheses is $H \geq 4$, the number of parameters of this reduced polar parameterization is shorter with respect to classical Cartesian one ($3 + H$ against $2H$ used in Cartesian parameterization). The advantage of this reduced polar parameterization with respect to the polar alternative presented in [40] is that it does not duplicate common hypothesis parameters x_i, y_i and ρ_i. Furthermore, unlike decentralized filters [25], the single state-vector-parameterization of nodes used in [26] allows the cross correlations between landmarks to be taken into account.

However, as in RO-SLAM the number of hidden variables to be estimated increases with the dimensionality of the problem, for the case of 3D RO-SLAM, it is necessary to increase the state vector of landmarks to estimate not only the azimuth angle of the landmark but also the elevation angle (see Fig. 1). A straightforward extension of previous polar parameterizations into spherical parameterization would consist of using a single GMM with multivariate Gaussian modes. Each mode would represent a single hypothesis with azimuth angle θ_i and elevation angle ϕ_i. Then, the 3D state vector of a range-only landmark with Cartesian (2) and the spherical (3) parametrization described would be:

$$
\begin{aligned}
f_i =\ & [x_{i1}, y_{i1}, z_{i1}, x_{i2}, y_{i2}, z_{i2}, ..., x_{iH}, y_{iH}, z_{iH}]^T & (2) \\
f_i =\ & [x_i, y_i, z_i, \rho_i, \theta_{i1}, \phi_{i1}, \theta_{i2}, \phi_{i2}, ..., \theta_{iH}, \phi_{iH}]^T & (3)
\end{aligned}
$$

Hence, the required number of parameters per landmark with a 3D Cartesian parameterization (2) would be $3n$ whereas with a spherical formulation using a single GMM (3) it would be $4 + 2H$, being H the number of hypotheses.

The reduced parameterization proposed by authors of this paper in [27] is based on a generalization of the spherical parameterization (3), which makes it suitable for different dimensionalities. This reduced parameterization, instead of representing all hypotheses with a single GMM, uses one GMM per hidden variable (i.e. in RO-SLAM, one GMM for each bearing parameter). Thus in the case of 3D RO-SLAM, hypotheses used to cover the spherical shell distribution shown in Fig.3 are parameterized using 3 parameters for the center $[x_i, y_i, z_i]^T$, another for the radius of the sphere ρ_i, N parameters to represent the azimuth angle samples (modes of the first GMM θ) and M parameters for elevation angle samples (modes of the second GMM ϕ). Thus, the number of parameters used for a landmark in 3D RO-SLAM would be $4 + N + M$, making the total number of hypotheses $H = N \times M$. In the case of 2D RO-SLAM, it would just use one GMM for the azimuth angle as in [26] with $4 + N$ parameters.

Then, for 3D parameterization, the complete state vector of a landmark i using this reduced parameterization would be:

$$f_i = [x_i, y_i, z_i, \rho_i, \theta_{i1}, ..., \theta_{iN}, \phi_{i1}, ..., \phi_{iM}]^T \tag{4}$$

Table 1 and Fig. 4 show a comparison in the number of parameters required to represent the spherical shell distribution shown in Fig. 1 with the 3D Cartesian, the single-GMM spherical and the reduced parameterization for different number of hypotheses. As can be seen, for example, to represent **1024 hypotheses** 3072 parameters are needed in the case of 3D Cartesian, 2052 in the case of the single-GMM spherical and only **68 parameters** with the proposed reduced parameterization (4 plus 32 azimuth + 32 elevation angles - Sect. 3 shows the details of state initialization).

However, the reduction of parameters in the reduced spherical parameterization limits the distribution of the hypotheses, i.e. while the azimuth and elevation samples are distributed uniformly on the range $0 - 2\pi$, the joint hypotheses distribution is not uniformly distributed. So, a good covariance should be used for the azimuth and elevation angles for each Gaussian to cover the entire spherical shell distribution of the
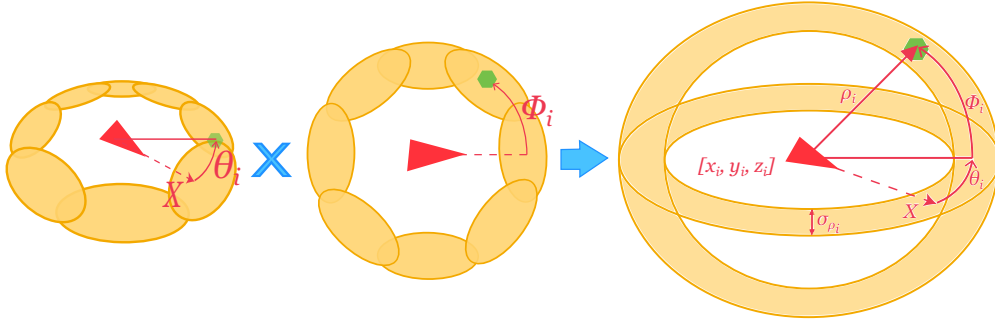
Figure 3: Reduced parameterization for 3D RO-SLAM: The combination of the GMM used for the azimuth angle with the GMM used for the elevation angle represent the set of hypotheses used to model the spherical shell distribution.
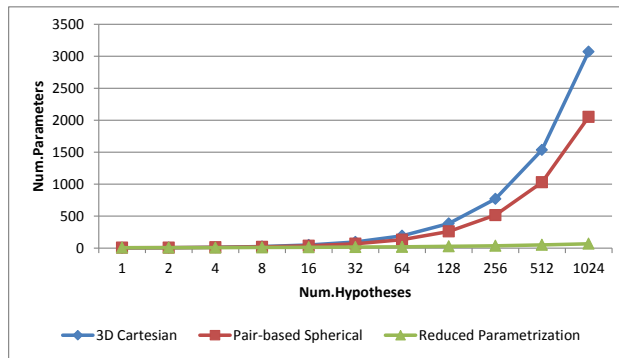

Figure 4: Number of parameters used to model a given quantity of hypotheses for the different 3D RO-SLAM parameterizations.

Table 1: Comparison of different parameterizations for 3D RO-SLAM.

#Hyp\#Params	3D Cart.	Spherical	Reduced
4	12	12	8
32	96	68	16
64	192	132	20
512	1536	1028	50
1024	3072	2052	68

landmark position. The way in which these covariance matrices should be computed during the initialization
stage of a landmark will be shown in the following section.

3. EKF-based 3D RO-SLAM

Most SLAM implementations, like visual SLAM (or bearing-only SLAM), tend to be more efficient when using a FastSLAM approach. This SLAM scheme is based on the Rao-blackwellization of the map and robot belief which makes an independence assumption between landmarks. However, although RO-SLAM might also be implemented with a FastSLAM making the same independence assumption, the high constraints introduced by inter-landmark observations in RO-SLAM are better modeled using an EKF. Hence, this paper uses a multi-hypotheses approach which integrates Gaussian Mixture Models (GMM) in an undelayed EKF-SLAM scheme based on [26] approach.

EKF-SLAM gathers the robot and landmarks parameters in a single state vector, using the covariance matrix to represent the cross correlations between robot and landmarks. The state vector of the proposed

EKF-SLAM for 3D RO-SLAM is composed of the following parameters:

$$\mathbf{x^t} = [\mathbf{x}_r^t, \mathbf{f}_1^t, \mathbf{f}_2^t, \ldots, \mathbf{f}_m^t]^T \tag{5}$$

where $\mathbf{x}_r^t$ is the robot state which follows a unimodal Gaussian distribution (e.g. $\mathbf{x}_r^t = [x_r^t, y_r^t, z_r^t]^T$) and $\mathbf{f}_i^t$ is the landmark i multi-modal Gaussian state.

The Extended Kalman Filter is based on the Markov independence assumption to implement the Gaussian bayesian filter used to compute the belief:

$$bel(\mathbf{x}^{t+1}) = p(\mathbf{z}^{t+1}|\mathbf{x}^{t+1}) \int p(\mathbf{x}^{t+1}|\mathbf{x}^t, \mathbf{u}^{t+1}) bel(\mathbf{x}^t) dx \tag{6}$$

where $\mathbf{u}^{t+1}$ is the last system action and $\mathbf{z}^{t+1}$ the last range-only observation. In the case of EKF, the prediction stage of bayesian filter is based on a marginalization of the current next state $\hat{\mathbf{x}}^{t+1}$ with respect last action $\mathbf{u}^{t+1}$ and previous state $\mathbf{x}^t$. Later, when the system receives new range-only observations $\mathbf{z}^{t+1}$, it computes the belief by computing the conditional probability $p(\mathbf{x}^{t+1}|\mathbf{z}^{t+1})$. The EKF equations for marginalization are formalized in the following expressions:

$$\hat{\mathbf{x}}^{t+1} = g(\mathbf{x}^t, \mathbf{u}^{t+1}) \tag{7}$$
$$\hat{\mathbf{P}}^{t+1} = \mathbf{G}\mathbf{P}^t\mathbf{G}^T + \mathbf{R} \tag{8}$$

where $\mathbf{G}$ is the Jacobian of the non-linear robot dynamic model $g(\mathbf{x}^t, \mathbf{u}^{t+1})$ and $\mathbf{R}$ is the noise matrix of the robot dynamic model. In this paper we will not focus on the prediction phase since any robot dynamic model used for other SLAM approaches can also be used for RO-SLAM, like the quadrotor dynamic model described in [41].

The update stage algorithm for the proposed RO-SLAM approach is summarized in Fig. 5. In the first step of this flow chart the reader may notice that range-only observations are pre-filtered before passing them to the EKF-SLAM framework. This pre-filtering is highly recommended to filter range-only outliers which might lead to EKF divergences. In this paper the pre-filtering technique described by authors of this paper in [38] is used, though other techniques might also be applied, like the one proposed in [24]. The other steps of the flow chart shown in Fig. 5 are detailed in the following subsections.

3.1. Landmark initialization

For initialization of new landmarks this paper proposes an adaptive scheme which adapts to the first range-only observation received at the current robot position. Thus, only range measurements between the robot and one landmark are considered for initialization as shown in Fig. 5. Landmarks located further than a certain distance threshold should be discarded to reduce the computational load, as range information worsen with distance normally.

New landmarks are initialized when the first range-only observation r_i is received by the robot from a landmark i. With this observation r_i and the current position of the robot $\mathbf{x}_r$, the parameters of (4) are initialized as:

$$\mathbf{x}_i = \mathbf{x}_r^t \tag{9}$$
$$\rho_i = r_i^t \tag{10}$$
$$\theta_{ij} = \frac{2\pi j}{N} - \pi \quad j = 1, \ldots, N \tag{11}$$
$$\phi_{ij} = \frac{\pi j}{M} - \frac{\pi(M+1)}{2M} \quad j = 1, \ldots, M \tag{12}$$

where $\mathbf{x}_i = [x_i, y_i, z_i]$ is the robot position at the time the range-only observation r_i is received.

With (11) and (12), N azimuth and M elevation Gaussian modes are uniformly distributed within ranges $(-\pi, \pi]$ and $(-\pi/2, \pi/2)$ respectively. However, the number of modes required to distribute all hypotheses in
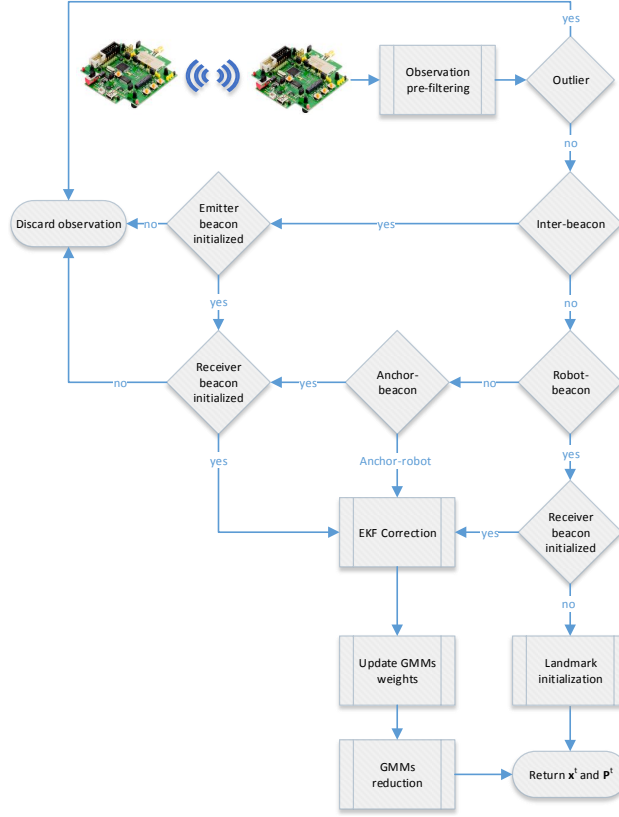
Figure 5: Flow chart describing the update stage of the proposed RO-SLAM algorithm upon receiving range measurements.

the spherical shell distribution depends on the radius of the sphere ρ_i and a desired density of hypotheses d (in practice $d = 0.18$ gives good results). Thus, the appropriate number of azimuth and elevation modes for both GMMs to cover the spherical shell distribution shown in Fig.1 might be computed from $H^* = 4\pi r_i^2 d$ as $H^* = N \times M$. Then, as hypotheses should be distributed with a spherical shell distribution, the number of elevation samples required are $M = N/2$ and hence the number of azimuth samples can be computed from the last two expressions as $N = \lceil \sqrt{2H^*} \rceil$. With this initialization strategy, the actual number of hypotheses generated is $H = N \times M \geq H^*$.

The next step is to initialize the covariance matrix of each Gaussian mode and their associated weights, $\omega_{\theta_{in}}$ and $\omega_{\phi_{im}}$. As both GMMs should approximate a uniform distribution around either the azimuth and elevation space, the values of $\omega_{\theta_{in}}$ and $\omega_{\phi_{im}}$ are easily initialized as $\omega_{\theta_{in}} = 1/N$ and $\omega_{\phi_{im}} = 1/M$.

The standard deviation of each variable of the state vector $\mathbf{f}_i$ is initialized as follows. The covariance matrix of parameters x_i, y_i and z_i is initialized using the current covariance of the robot position. The variance of ρ_i is initialized using the standard deviation of the range measurement as $\sigma_{\rho_i}^2 = \sigma_{r_i}^2$. Cross correlations with this variable are set to 0. Finally, the standard deviation of each Gaussian mode θ_{in} and ϕ_{im} is identically initialized for each GMM according to the following expressions, setting initial cross correlations to 0:

$$\sigma_{\theta_{in}} = \frac{2\pi}{k_\theta N} \quad n = 1, \dots, N \tag{13}$$

$$\sigma_{\phi_{im}} = \frac{\pi}{k_\phi M} \quad m = 1, \dots, M \tag{14}$$

where values k_θ and k_ϕ of the expressions (13) and (14) are proportional factors computed using the Kullback-
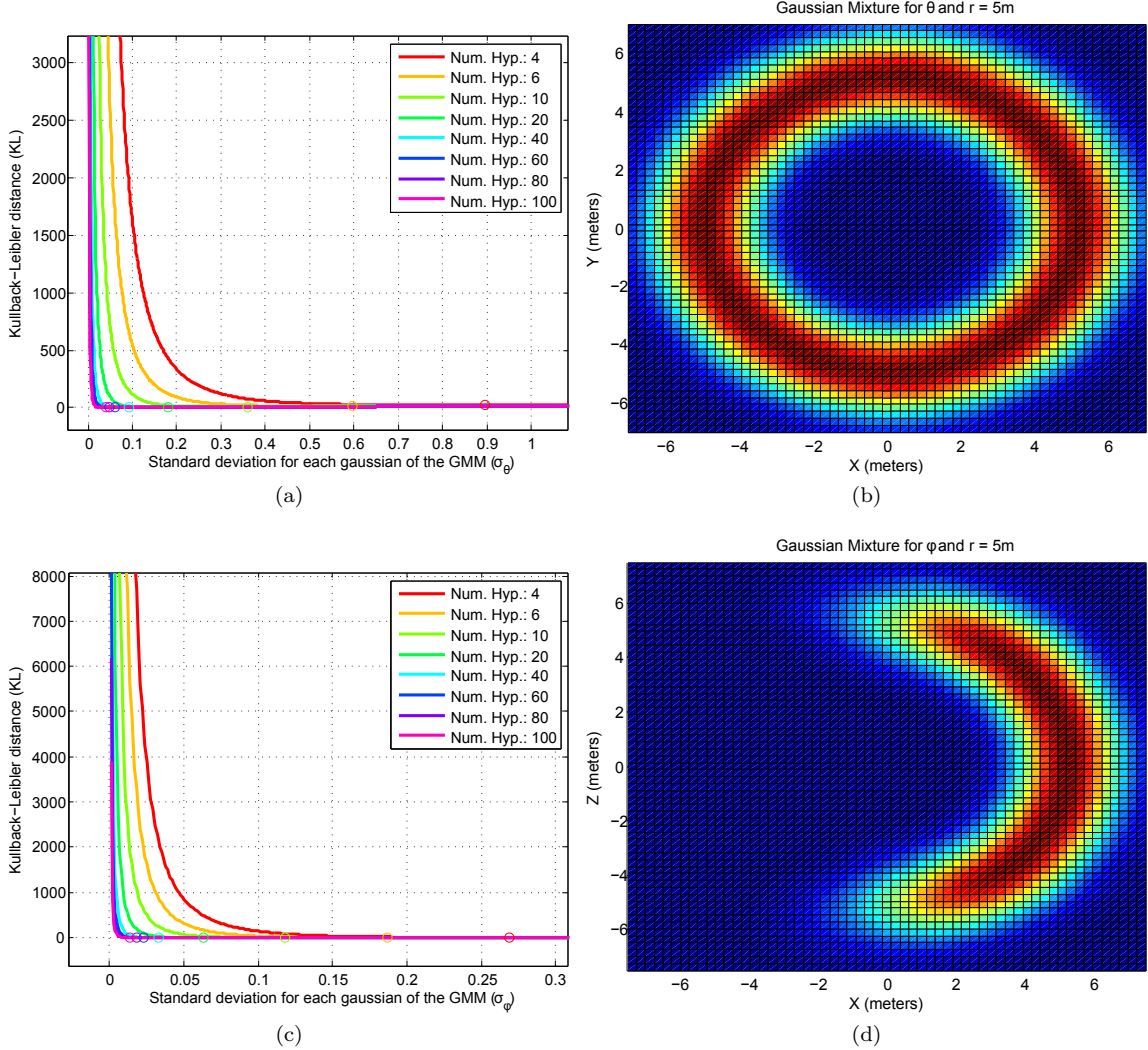
9

Figure 6: Experiments performed for the optimal selection of k_θ and k_ϕ factors. In (a) and (c) the Y axis represents the Kullback-Leibler divergence factor and the X axis represents the standard deviation used for each simulated GMM. Each series represents the simulation for a fixed number of modes in the GMMs. (b) and (d) shows an example of the GMM generated using the optimal values of K_θ and K_ϕ respectively. The combination of both GMM, (b) and (d), gives the uniform spherical shell distribution for a range measurement $r = 5m$ received at coordinates $[0, 0, 0]$.

Leibler (KL) distance between a Gaussian Mixtures and a target uniform distributions for θ_i and ϕ_i variables. The KL divergence factor is a statistic which comes from information theory and measures the amount of additional information that is required to model a target distribution (in this case the uniform distribution) given a proposal distribution (in this case a Gaussian Mixture). However, this statistic does not have a closed form for Gaussian Mixtures, hence a Monte Carlo sampling method [42] can be used to get an approximation of this statistic. When comparing two probability distributions, the best fit is that which has a information divergence (KL distance) equal to 0. Then, k_θ and k_ϕ were computed from a set of simulations where different Gaussian Mixtures with different number of modes were used to model a uniform distribution over $(-\pi, \pi]$ for k_θ and $(-\pi/2, \pi/2)$ for k_ϕ. For each Gaussian Mixture with k modes, different standard deviations were tested to initialize each mode of the Gaussian Mixture. The standard deviations which had the KL distance closest to 0 were selected as the optimal deviation for a given Gaussian Mixture with k modes.

10

These values are marked with circles in Fig. 6a and Fig. 6c. The selected standard deviations were used to get the mean value of k_θ and k_ϕ using the expressions (13) and (14). The results of these experiments are depicted in Fig. 6a and Fig. 6c, where the X axis represents the different standard deviations used for each Gaussian Mixture with k modes and the Y axis represents the KL distance. The values that gave the best fit were $k_\theta = 1.7$ and $k_\phi = 2.5$. Fig. 6b and Fig. 6d shows an example of the GMM generated for a range measurement of $r = 5m$ received at position $[0, 0, 0]$ using the initialization strategy explained in this section and proportional factors k_θ and k_ϕ. The combination of both GMMs, Fig. 6b and Fig. 6d, results in a uniform spherical shell distribution.

3.2. EKF and weights update

This section focuses on the correction stage of the EKF for range-only observations. The correction stage of a EKF computes the conditional probability $p(\mathbf{z}^{t+1}|\hat{\mathbf{x}}^{t+1})$ using the following common EKF correction equations:

$$
\begin{aligned}
\mathbf{x}^{t+1} &= \hat{\mathbf{x}}^{t+1} + \mathbf{K}(\mathbf{z}^{t+1} - h(\hat{\mathbf{x}}^{t+1})) \\
\mathbf{P}^{t+1} &= (\mathbf{I} - \mathbf{KH})\hat{\mathbf{P}}^{t+1}
\end{aligned}
$$

(15)

(16)

where $\mathbf{K}$ is the Kalman gain computed as $\mathbf{K} = \hat{\mathbf{P}}^{t+1}\mathbf{H}^T(\mathbf{H}\hat{\mathbf{P}}^{t+1}\mathbf{H}^T + \mathbf{Q})^{-1}$, and H is the Jacobian of the observation model $h(\mathbf{x}^t)$.

In this section only robot to landmark i observations (denoted as r_i) are considered, the next subsection will detail the correction scheme for range-only observations between two static range-only sensors u and v (denoted as r_{uv}).

Once a landmark $\mathbf{f}_i$ has been initialized using the first range-only observation, new observations r_i are used to correct the state vector of the EKF and the weights of GMMs for landmark i. Classical multi-hypothesis approaches use one correction equation per hypothesis (i.e. $N \times M$ equations) using Federated Information Sharing approach [1, 26, 27]. This approach is referenced here as **Full Hypotheses Correction (FHC)**. In the authors' previous work [27], a correction scheme is proposed which reduces the required number of correction equations from $N \times M$ to $N + M$ with respect to classical FHC approaches, this method is referred to here as **Multi-Hypotheses Correction (MHC)**. This correction scheme reduces the computational load of the innovation (or residual) matrix inversion in EKF, the dimensionality of which depending on the number of correction equations. In this paper, this correction scheme is improved with a small reduction of accuracy to a single correction equation using a novel technique which the authors have called Gaussian Mixture Correction (GMC). By using this technique, the inversion of the innovation matrix becomes a scalar inversion when receiving a single range measurement at time t. The technique consists on the integration of the complete GMMs in the correction equation by using the expectation of each Gaussian Mixture, so the weights of the GMMs are taken into account as constant variables when correcting the landmark hypothesis states. The expectation (or overall mean) of a Gaussian Mixture GMM with k Gaussian modes $\mathcal{N}(\mu_i, \sigma_i)$ is computed as [43]:

$$
E[GMM] = \sum_{i=1}^{k} \omega_i \mu_i
$$

(17)

Using GMC in 3D RO-SLAM is as easy as using the expectation of the azimuth $E[\theta_i] = \theta_i$ and elevation $E[\phi_i] = \phi_i$ GMMs in the non-linear observation model of range measurements. The integration of expectations θ_i, ϕ_i in the range-only observation model for the linearization point $\mathbf{x} = [x_r, y_r, z_r, x_i, y_i, z_i, \rho_i, \theta_i, \phi_i]$ can be formulated as:

$$
h(\mathbf{x}) = \sqrt{\delta_x^2 + \delta_y^2 + \delta_z^2}
$$

(18)

11

where $\delta_x = (x_{f_i} - x_r)$, $\delta_y = (y_{f_i} - y_r)$, $\delta_z = (z_{f_i} - z_r)$ and x_{f_i}, y_{f_i} and z_{f_i} stand for:

$$\begin{aligned}
x_{f_i} &= x_i + \rho_i cos(\theta_i)cos(\phi_i) \\
y_{f_i} &= y_i + \rho_i sin(\theta_i)cos(\phi_i) \\
z_{f_i} &= z_i + \rho_i sin(\phi_i)
\end{aligned} \tag{19}$$

Notice that the use of this observation model for 2D RO-SLAM, in contrast to the MHC method used in [26], is similar to 3D RO-SLAM but omits altitude terms z and with a fixed elevation value $\phi_i = 0$ in (18) and (19).

With this correction scheme, it is no longer necessary to split the variance of the range measurement among multiple equations using Federated Information Sharing approach. In general, including the weights of GMMs in the observation model $h(\mathbf{x})$ makes it more informative than MHC method, allowing a faster convergence in the filter. With GMC approach all hypotheses are equally affected when they are uniformly distributed (i.e. all hypotheses have the same weight) but, as the weights are updated, those hypotheses with higher likelihood are favored, making the whole GMMs converge to the most probable hypotheses. GMC not only reduces the computational load required in the correction stage of multi-modal observation models but also eases the implementation of multi-hypothesis solutions with respect other similar methods in the literature.

However, the efficiency and simplicity of this correction scheme comes at expense of a possible initial reduction in the accuracy of the correction scheme with respect to other approaches. This small loss of accuracy only happens in those cases where the initial GMM distributions make the Jacobian (18) linearization point be far from the actual position of the landmark since this linearization point is computed as the expectation value of each GMM. However, as will be shown later, this correction scheme compensates this loss of accuracy by accelerating the convergence time of hypotheses with respect to other approaches and hence makes the linearization point converge to the real landmark position with only a few range-only observations.

After the EKF state has been corrected, the weights $\omega_{\theta_{in}}$ and $\omega_{\phi_{im}}$ of both GMMs must be updated according to the current distribution of $p(r_i|\mathbf{x}_r^{t+1}, \mathbf{x}_i^{t+1}, \rho_i, \theta_i, \phi_i)$. However, $\omega_{\theta_{in}}$ and $\omega_{\phi_{im}}$ depends on the following marginal probabilities:

$$\begin{aligned}
\omega_{\theta_{in}}^{t+1} &= \omega_{\theta_{in}}^{t} p(r_i^{t+1}|\mathbf{x}_r^{t+1}, \mathbf{x}_i^{t+1}, \rho_i^{t+1}, \theta_{in}^{t}) \tag{20}
\end{aligned}$$

$$\begin{aligned}
\omega_{\phi_{im}}^{t+1} &= \omega_{\phi_{im}}^{t} p(r_i^{t+1}|\mathbf{x}_r^{t+1}, \mathbf{x}_i^{t+1}, \rho_i^{t+1}, \phi_{im}^{t}) \tag{21}
\end{aligned}$$

To compute these marginal distributions, this paper propose to use the following equations based on an independence between landmark parameters as in [27] but using the Total Probability Theorem for discrete random variables [30]. This method is referenced along this paper for comparison purpose as Total Probability Update (TPU):

$$p(r_i|\mathbf{x}_r, \mathbf{x}_{\theta_{in}}) = \sum_{m=1}^{M} p(r_i|\mathbf{x}_r, \mathbf{x}_{\theta_{in}}, \phi_{im})p(\phi_{im}) \tag{22}$$

$$p(r_i|\mathbf{x}_r, \mathbf{x}_{\phi_{im}}) = \sum_{n=1}^{N} p(r_i|\mathbf{x}_r, \mathbf{x}_{\phi_{im}}, \theta_{in})p(\theta_{in}) \tag{23}$$

where $\mathbf{x}_{\theta_{in}} = [\mathbf{x}_i, \rho_i, \theta_{in}]$, $\mathbf{x}_{\phi_{im}} = [\mathbf{x}_i, \rho_i, \phi_{im}]$, $p(\theta_{in}) = \omega_{\theta_{in}}^{t}$ and $p(\phi_{im}) = \omega_{\phi_{im}}^{t}$. Conditional probabilities $p(r_i|\mathbf{x}_r, \mathbf{x}_{\theta_{in}}, \phi_{im})$ and $p(r_i|\mathbf{x}_r, \mathbf{x}_{\phi_{im}}, \theta_{in})$ are evaluated as Gaussian distributions, with mean computed with (18) for each hypothesis composed by θ_{in} and ϕ_{im} modes, and variance $\sigma_{r_i}^2$.

TPU has the same computational complexity as the method proposed in [27], which is referenced in this paper as Maximum Likelihood Update (MLU). The difference with MLU, is that TPU considers the complete multi-modal distribution of the azimuth and elevation angles instead of using the most probable

Gaussian mode, making the method more robust against noisy measurements. The main advantage of considering azimuth and elevation samples as independent variables is that the weights of these parameters can be stored with a storage complexity $O(N + M)$ against the storage complexity required to store each joint hypotheses weight $O(N \times M)$. The reduced spherical parameterization proposed in this paper might be used with the weights update strategies MLU and TPU. However, as neither the reduced parameterization nor the new GMC observation model imply an independence between azimuth and elevation angles, the parameterization might also be used with classical update strategies used in the literature by storing the joint hypotheses weights instead of storing the weights of azimuth and elevation samples independently.

3.3. Inter-node range-only observations

Previous paragraphs have described the observation model employed to correct the EKF state using robot to landmark range-only observations. However, as Fig. 5 shows, there are two additional types of range-only observations, namely those measured between static landmarks (also called inter-node observations), i.e. those generated from one anchor (range-only sensors which position is given) to one landmark and those generated between 2 landmarks (also called inter-node range-only observations).

For the case of anchor-landmark range-only observations $r_{A_i u}$, the observation model of these measurements is quite similar to (18) but with $\delta_x = (x_{f_i} - x_{A_i})^2$, $\delta_y = (y_{f_i} - y_{A_i})^2$ and $\delta_z = (z_{f_i} - z_{A_i})^2$. Thus, in this case, as the robot state vector x_r is not used, and $\mathbf{x}_{A_i}$ is not part of the state vector, the first terms of jacobian relating to the robot position would be $\frac{\partial h(\mathbf{x})}{\partial \mathbf{x}_r} = 0$. On the other hand, the conditional probability used to update the weights of the GMMs are no longer conditionally dependent on the robot position but on the fixed position of the anchor $\mathbf{x}_{A_i}$ and will be computed again using TPU:

$$\omega_{\theta_{in}}^{t+1} \quad = \omega_{\theta_{in}}^t p(r_i^{t+1}|\mathbf{x}_{A_i}, \hat{\mathbf{x}}_i^{t+1}, \rho_i^{t+1}, \theta_{in}^t) \tag{24}$$

$$\omega_{\phi_{im}}^{t+1} \quad = \omega_{\phi_{im}}^t p(r_i^{t+1}|\mathbf{x}_{A_i}, \hat{\mathbf{x}}_i^{t+1}, \rho_i^{t+1}, \phi_{im}^t) \tag{25}$$

In the case of inter-landmark range-only observations r_{uv}, this paper proposes to use (18) but with $\delta_x = (x_{f_u} - x_{f_v})^2$, $\delta_y = (y_{f_u} - y_{f_v})^2$ and $\delta_z = (z_{f_u} - z_{f_v})^2$.

The probability distribution functions employed to update the weights of both landmarks' GMMs are:

$$\omega_{\theta_{un}}^{t+1} \quad = \quad \omega_{\theta_{un}}^t p(r_{uv}^{t+1}|\mathbf{f}_v^{t+1}, \mathbf{x}_u^{t+1}, \rho_u^{t+1}, \theta_{un}^{t+1}) \tag{26}$$

$$\omega_{\phi_{um}}^{t+1} \quad = \quad \omega_{\phi_{um}}^t p(r_{uv}^{t+1}|\mathbf{f}_v^{t+1}, \mathbf{x}_u^{t+1}, \rho_u^{t+1}, \phi_{um}^{t+1}) \tag{27}$$

$$\omega_{\theta_{vn}}^{t+1} \quad = \quad \omega_{\theta_{vn}}^t p(r_{uv}^{t+1}|\mathbf{f}_u^{t+1}, \mathbf{x}_v^{t+1}, \rho_v^{t+1}, \theta_{vn}^{t+1}) \tag{28}$$

$$\omega_{\phi_{vm}}^{t+1} \quad = \quad \omega_{\phi_{vm}}^t p(r_{uv}^{t+1}|\mathbf{f}_u^{t+1}, \mathbf{x}_v^{t+1}, \rho_v^{t+1}, \phi_{vm}^{t+1}) \tag{29}$$

In this case, conditional probabilities of (26)-(29) are again computed using Total Probability Theorem over variables ϕ_{um}, θ_{vn} and ϕ_{vm} for (26), variables θ_{un}, θ_{vn} and ϕ_{vm} for (27), variables ϕ_{vm}, θ_{un} and ϕ_{um} for (28) and variables θ_{vn}, θ_{un} and ϕ_{um} for (29).

The update of landmarks' GMMs weights might be computationally expensive in cases of inter-landmark observations when these landmarks contains a high number of hypotheses, however, in practice, as landmarks are static, this observations can be integrated in the EKF at a low frequency to avoid filter overconfidence regarding the landmarks positions. On the other hand, as will be shown during experimental validation, inter-landmark observations, together with robot-landmark measurements, make the hypothesis convergence faster. Thus, once landmarks converge to a single hypothesis, the application of (26)-(29) is as expensive as integrating a range measurement between two positions, situation in which the weights do not need to be updated.

3.4. GMMs Reduction

As in other multi-hypothesis methods, it is highly recommended to prune hypotheses as they become less probable or merge those similar. This reduction lowers the computational burden of multi-hypothesis

methods which, in this case, only affects the length of the state vector but not the correction stage of the EKF as commented above. The heuristics used in this paper to reduce the number of modes of one GM are based on the following rules:

- If a mode weight ω_{ij} is lower than a certain threshold δ_{th} then, the mode j is pruned. The threshold used here is $\delta_{th} = 10^{-11}/k$, where k is the current number of modes in the Gaussian Mixture. The value 10^{-11} has been selected experimentally looking for a trade-off between accuracy and efficiency.

- The second rule is used to merge similar modes. Two modes of the same GM are merged if their relative arc distance $\rho_i|\alpha_{in} - \alpha_{im}|$ is bellow a certain threshold δ_d (in practice $\delta_d = 0.25m$ gives good results), here α_{ij} represents two different modes of a single Gaussian Mixture (the azimuth or the elevation GMM). In order to merge two similar modes, this section use the moment-preserve merge procedure explained in [43] because, as its name suggests, it preserves the overall moment of the Gaussian Mixture when merging two modes as compared to other methods [26, 27] which prune the one with lower weight without preserving the overall moment.

As might be noticed, as a consequence of the reduced parameterization proposed here, after pruning a Gaussian mode θ_{in} from the θ_i GMM, actually M full hypotheses are pruned from the spherical shell distribution (in the same way, N full hypotheses are deleted when pruning a mode ϕ_{im}).

4. Results

This section is aimed at validating the different contributions of the RO-SLAM algorithm presented in this paper. First, some simulations are used to compare the map scalability, the observation models and the weights update strategies with respect to state-of-the-art RO-SLAM approaches. As the reader may notice, there is not too much work on online 3D RO-SLAM, so the classical 3D RO-SLAM algorithms described above have been implemented in ROS framework for comparison purposes. On the other hand, the results on a real dataset will be compared with a previous algorithm by the authors [27] based on MHC and MLU. Finally, a comparison of RO-SLAM accuracy with and without inter-node range-only observations is presented using simulated and real experiments. A video for one of the real experiments described below is available (see Fig.9) showing the results of the algorithm described in this paper on indoor environments (FADA-CATEC testbed shown in Fig.9a) with a real aerial robot.

The methods presented in this paper and other state-of-the-art algorithms have been implemented in C++ using the Robot Operating System (ROS) framework. During simulations, the simulated aerial robot used is based on the hector model from one of the ROS packages. Simulated range-only sensors are based on the characterization of range-only sensors used for real experimentation. These sensors are radio-based range-only sensors (also called nodes) with a 0 mean error with standard deviation of 0.5 meters at 70Hz, which is similar to the characteristic of the range measurements generated by a real Nanotron range sensor as shown in Fig.7b. Typically range measurements are limited to a maximum distance as the number of outliers increase linearly with the distance between the range-only sensors as it is shown in Fig.7a.

During the real experiments, a Pelican quadcopter from Asctec was used with an onboard radio-based range-only sensor (base node) from Nanotron [44] (see Fig. 9c). It is well-known that precise odometry is complex in aerial robots and hence, in order to localize the robot during these experiments, a set of static sensor nodes with known position (anchors) were used to localize the robot. Some aerial robots use visual odometry to cope with this problem [45]. In this paper, anchors allow the aerial robot to be localized by multilateration of the robot position by using range measurements taken from the robot to the anchors. Even though a precise prediction model might improve the results of the experiments presented in this paper, a simple prediction model has been implemented for these experiments which just increases the variance of robot parameters with a very small value at a high frequency. At least 4 anchors are required to estimate the three-dimensional position of the aerial robot. The range-only sensor is based on a development board and has the following characteristics:

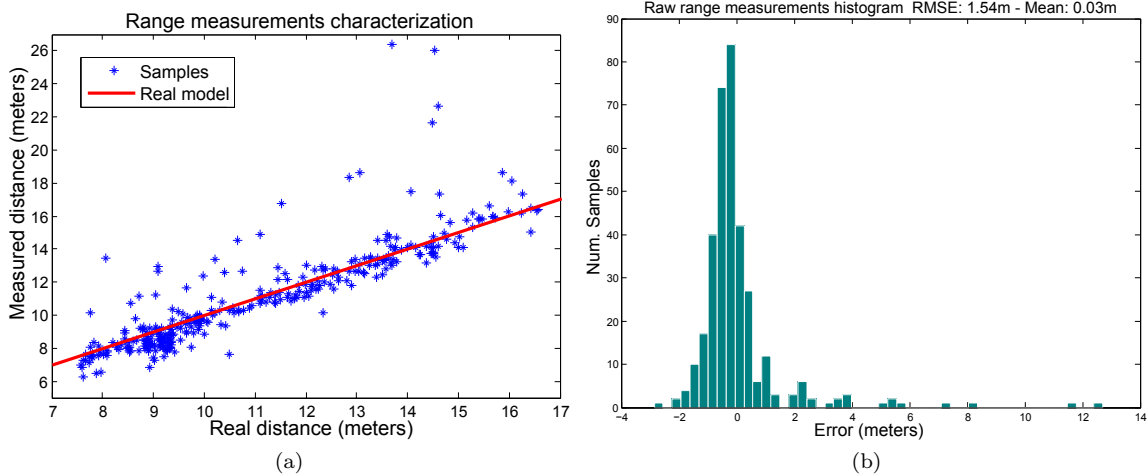- General purpose ATMega 1284P microcontroller at 20MHz.

14

Figure 7: Nanotron range-only sensor characterization for indoor environments: (a) sensor characterization (b) error histogram.

- Radio transceiver 2.4 GHz ISM band. Up to 20dB transmission power.

- Ranging accuracy of **2 m indoors** / 1 m outdoors.

- 128KB flash memory for programs and retrieved data.

- Distance measurements computed with the SDS-TWR method, based on the ToF method but without needing any clock synchronization between nodes.

An example of the pre-filtering [46] results for range-only observations between robot (node 25) and node 6 is shown in Fig.8 for a Nanotron radio-based range-only sensor in a real indoor experiment. The results of the pre-filtering method are compared with the real distance between nodes 25 and 6. The real distance of mobile node 25 is measured using the ground truth of the robot and the static node 6. Both ground truths were measured using a VICON motion-tracking system (see Fig. 9b). This figure shows how this filter not only smooths the raw range-only observations (blue line) but also rejects most range outliers. With this pre-filtering method, the filtered range-only observations (red line) get closer to the real distance measured between nodes 25 and 6 (green line).

Additionally, to complement the poor trilateration of the aerial robot altitude, the onboard barometric altimeter of the Pelican was used, including the estimation of the altimeter bias in the EKF (the equations of the altimeter bias have been omitted because it is out of the scope of this paper). The simulator generates altitude measurements with a mean error biased throughout the time of the experiment and with a standard deviation of 20mm at a frequency of 20Hz (similar to the barometric barometric altimeter sensor used in real experiments).

4.1. Simulation results

Simulation results are mainly used for comparison purposes between the proposed method and other methods in the literature. The first experiments compare the scalability and accuracy of the proposed reduced spherical parameterization (or RSP) against other classical parameterizations. Later, the GMC observation model is compared with other models based on Federated Information Sharing. The independence assumption made between azimuth and elevation parameters in MHU and TPU strategies will be validated by comparing the results with the common joint hypothesis weight update strategy where azimuth and elevation parameters are considered as dependent random variables. As the main objective of these experiments is to evaluate the mapping algorithm proposed for RO-SLAM, during simulation experiments the position of the robot is given to avoid mapping errors coming from a bad localization of the aerial robot. Real experiments will evaluate the complete SLAM approach showing localization and mapping results.
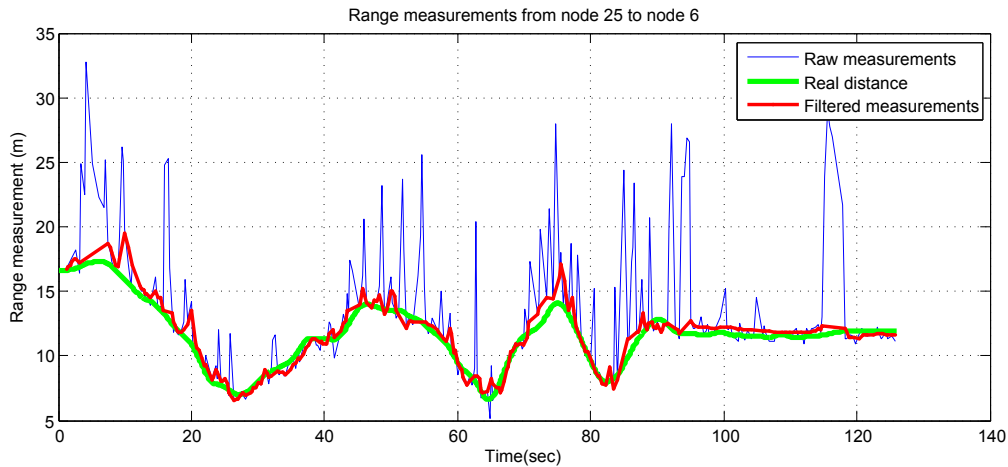
15

Figure 8: Pre-filtering results for real range-only observations taken with a radio-based range-only sensor. Filtered range measurements (red line) are plotted along with raw observations (blue line) and real distances (green line).

4.1.1. Map scalability

The scalability is validated using different simulations for up to 50 landmarks randomly distributed in a region of 30 x 30 x 10 meters comparing the computational complexity and accuracy of the mapping approaches using the large spherical parameterization (LSP) extended from [26], the 3D Cartesian parameterization used in [37] and the reduced parameterization proposed in [27].

In Fig. 4 (shown above) a large improvement in the amount of parameters required to estimate the same number of hypotheses with respect to other classical EKF representations was demonstrated. As stated in [30], it is well known that the computational complexity of the EKF framework is directly related with the number of parameters, thus the reduction of the state vector implies an improvement in the EKF-SLAM framework. This theoretical results on computational complexity are validated with the simulation results shown in Fig. 10a. This figure shows the maximum processing time spent during the correction stage of the EKF, i.e. during computation of equations (15) and (16). The maximum processing time is used since in most of the cases it coincides with the case of a maximum number of parameters in the state vector. On the other hand, Fig. 10b shows the average mapping error for different number of beacons. As can be seen, the mapping error is approximately the same for all parameterizations but a clearly computational complexity reduction is shown in the case of the reduced parameterization shown in Fig. 4. Another characteristic of the mapping error is how it increases with the number of landmarks which is mainly related with a reduced convergence time of the solution due to the inter-landmark correlations introduced by EKF.

In this case, the scalability is studied with the number of landmarks (or beacons). However, the same results might be reached by using just one beacon and increasing the initialization distance or the density of hypotheses d.

4.1.2. Observation model

The following simulations are aimed at comparing classical observation models used in centralized EKF-SLAM approaches based on Federated Information Sharing [1, 26, 27] (FHC or MHC methods) with the observation model proposed here (GMC). As there is no open implementation of FHC method for 3D RO-SLAM, this method has also been implemented in C++ along with MHC and GMC methods for the sake of method comparison and benchmarking. For all these observation models the proposed reduced spherical parameterization is used to demonstrate how this parameterization can also be used with classical observation models. In this case, the results are compared against different initialization densities d (i.e. different number of hypotheses per beacon) and with a fixed number of 10 beacons. The idea is to compare the processing time with a larger number of correction equations in the observation model and also with a different number of parameters in the state vector.
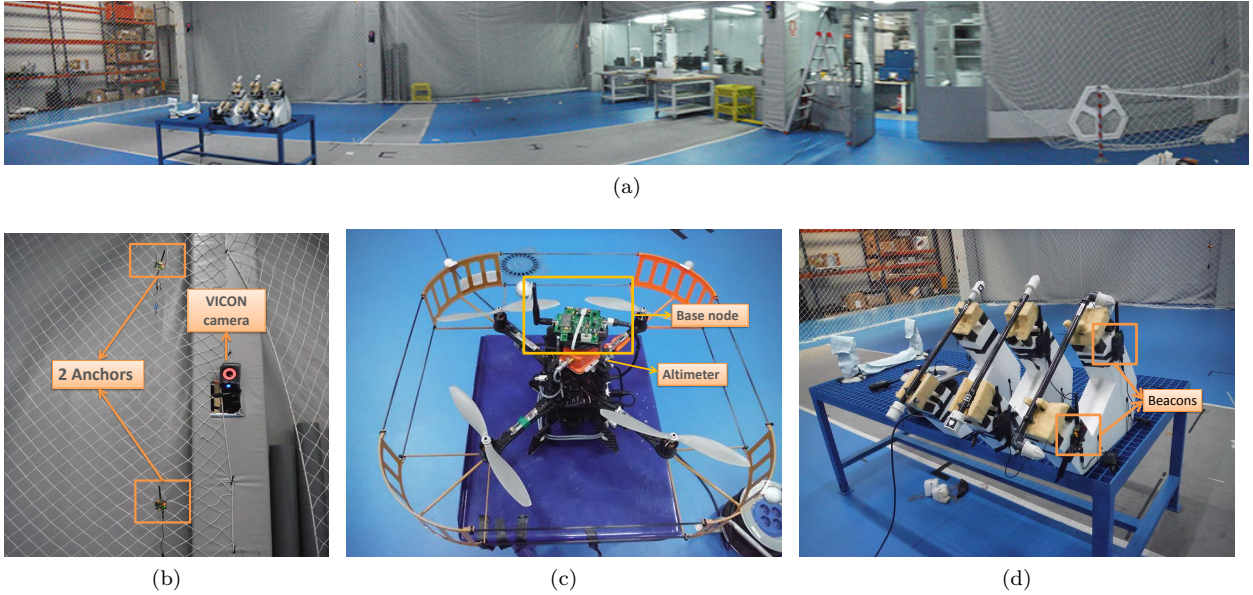
16

Figure 9: Setup used for indoor real experiments: (a) FADA-CATEC indoor testbed (b) anchors used for localization and VICON system used for groundtruth (c) Pelican aerial robot from Asctec (d) 3 bars with 6 embedded beacons. Video available at http://grvc.us.es/staff/caba/share/video.mp4

As shown in equation (16), the computational burden on the inversion of the innovation matrix depends on the number of correction equations whereas the rest depends on the number of parameters in the state vector. Fig. 11a shows the processing time taken not only in the correction stage of the EKF but also in computing the matrices of the range-only observation model (Jacobian, noise matrix, etc). The figure shows a quadratic increase for FHC due to the quadratic dependence with the number of azimuth and elevation angles while the other models are more linear. In the case of GMC the linear increment on the processing time is because of the increment in the number of parameters on the state vector. MHC depends not only on the number of parameters to model all hypotheses but on the number of correction equations used. On the other hand, Fig. 11b shows GMC has a faster convergence rate for reaching a single hypothesis compared to the other models coming at the expense of the worst mapping error as shown in Fig. 11c. As this last figure shows, the mapping error decreases as the density of hypotheses increases during initialization phase. This decrease is lower for FHC and higher for MHC.

4.1.3. Weights update

Despite the convergence time of beacons depends very much on the observation model implemented (FHC, MHC or GMC), it is mainly related with the strategy used to update the weights of GMMs. The correction strategies MHC and GMC can be combined with different methods used to update the weights of GMM (e.g. MHC with MLU or MHC with TPU, etc). However, as MLU and TPU are based on the assumption that azimuth and elevation angles are independent, the classical Cartesian and LSP parameterizations are not suitable for these update strategies. On the other hand, as the reduced parameterization does not impose an independence between beacon parameters, this parameterization and the GMC observation model proposed here can be still used with the classical approach used to update the weights of hypotheses at expenses of a higher memory consumption. The following experiments compare the classical Full Hypotheses Update (FHU) strategy used in the literature [47, 26, 1] for dependent azimuth and elevation parameters with the methods proposed by authors of this paper, Most Likely Update (MLU) and Total Probability Update (TPU). In these experiments 10 beacons are used and the observation model used in these experiments is GMC.

In this case, the results are also compared against different hypotheses densities d to check the update

17
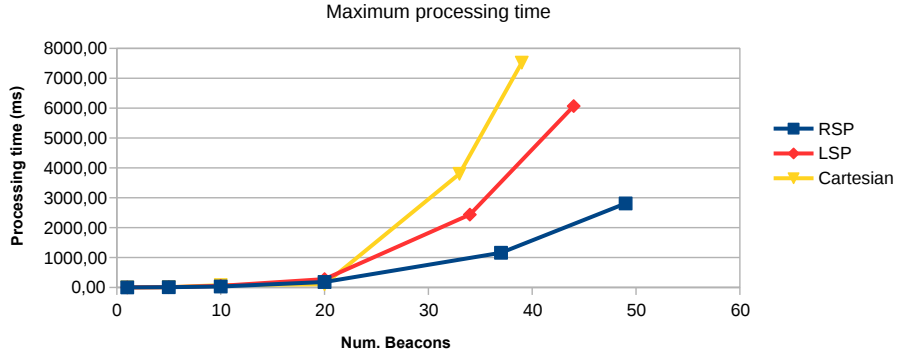
(a)
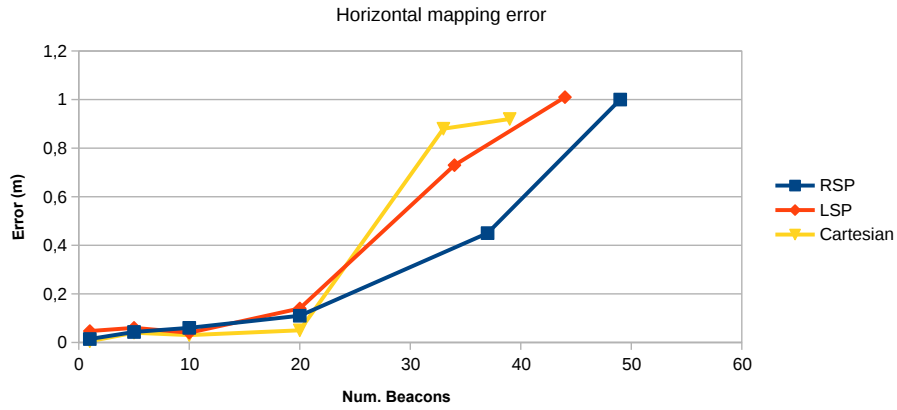
(b)

Figure 10: Comparison of the processing time and mapping error for the proposed Reduced Spherical Parameterization (RSP), the Large Spherical Parameterization (LSP) and the classical Cartesian parameterization: (a) EKF correction stage maximum processing time, (b) averaged mapping error.

processing time and the hypotheses convergence for the different strategies with a larger number of hypotheses per beacon. The processing time measured is the time used to update the weights of the Gaussian Mixtures plus the processing time taken by the prune strategy explained above.

As Fig. 12 there is not much difference between FHU and TPU methods and both have better performance than MLU. However, TPU tends to be the most efficient in terms of processing time and memory consumption. FHU consumes an amount of memory quadratic in the number of azimuth and elevation angles as explained above due to the dependence assumption made between landmark parameters. Additionally, the independence assumption does not seem to affect the accuracy of the mapping results when using either MLU or TPU.

4.2. SLAM accuracy

For real experimentation, 6 beacons embedded in 3 bars (2 beacons per bar) were used as shown in Fig. 9d. In this experiment, only MHC and GMC observation models are compared using MHC with MLU as the RO-SLAM algorithm presented in [27] against the algorithm proposed in this paper using GMC with TPU. The results obtained with this real dataset are shown in Fig. 14. The averaged localization error is 0.54 meters and the averaged mapping error is 0.6 meters with an averaged horizontal error of 0.14
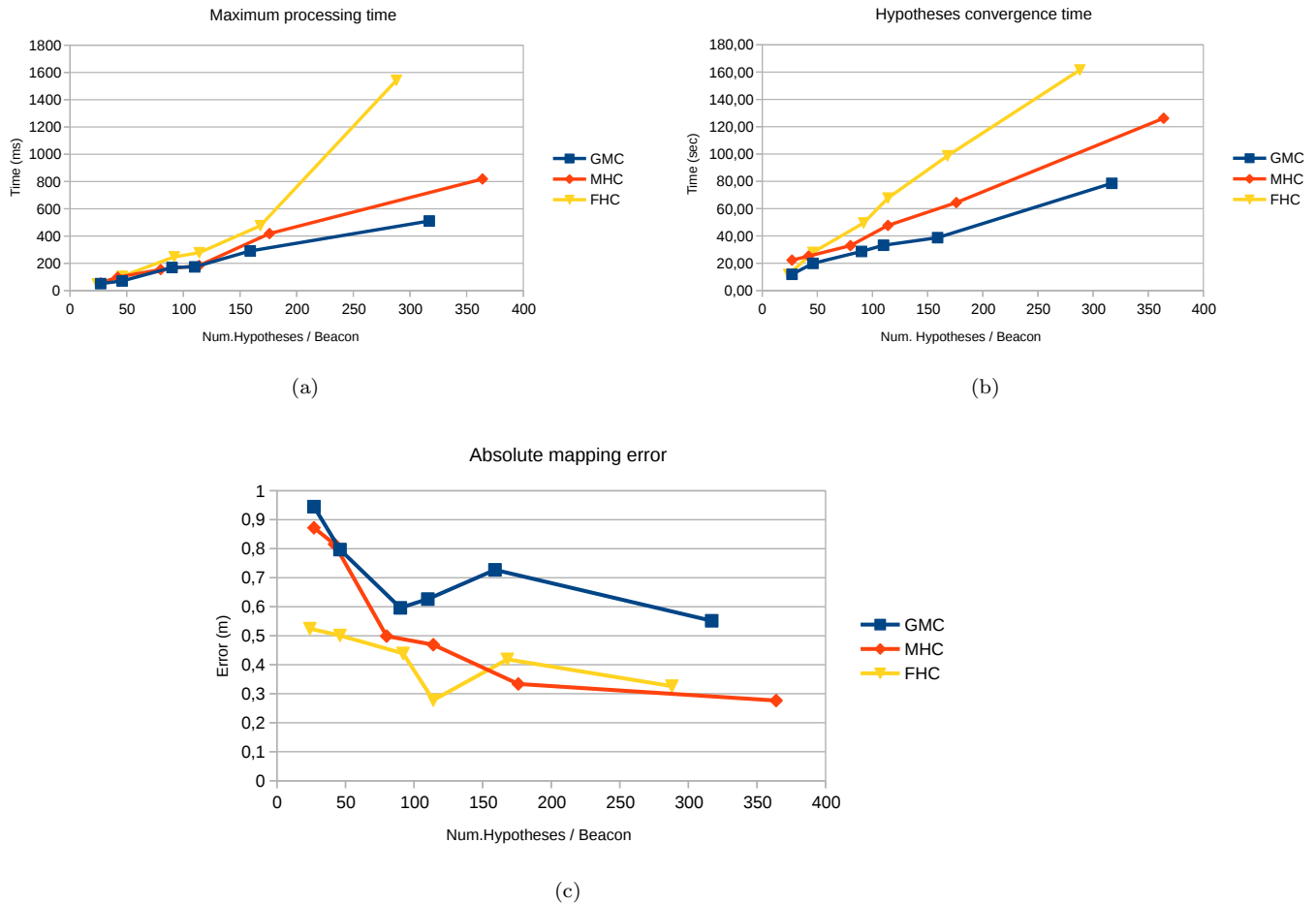
18

Figure 11: Comparison of (a) the processing time, (b) hypotheses convergence time and (c) averaged absolute mapping error for 10 beacons, different number of hypotheses and different range-only observation models.

meters for the MHC method, whereas for the GMC method the localization error is 0.54 meters and the averaged mapping error is 0.58 meters with an averaged horizontal error of 0.2 meters. Figure 13a shows the localization results for GMC (the MHC results are similar). As shown in Fig. 15 with a red line, 75% of the time the localization error is below 0.6 meters when not using inter-node range-only observations. Furthermore, as Fig. 13b shows with a green dashed line, the localization estimation shown in blue is always within the 3σ variance interval with respect the ground-truth of the aerial robot shown with a red line. As can be seen, the vertical error (Z axis) is higher than horizontal axis. The trilateration of the altitude is affected by this lack of movement and distribution of sensors position along this axis on tis real experiment.

Mapping error is shown in Fig.14a for MHC and in Fig. 14b for GMC. In this case, as it was an indoor experiment, the aerial robot only could fly in a range of 1.5-3 meters which is why the mapping error presents a higher vertical mapping error. This is specially notable in the case of beacon 22 because of a lack of observability in the beacon altitude. Again, the SLAM results are quite similar in both methods with a mapping error below 0.5 meters but with a reduced computational complexity in the case of GMC.

4.3. Inter-node range-only observations

This section validates the observation model for inter-node range-only observations in the EKF-SLAM framework described above. The same synthetic and real datasets used before are reused now but inter-

landmark observations are integrated. Inter-landmark measurements r_{ij} are filtered so that they are integrated in the filter at a frequency of 0.1Hz for the same pair of sensors i and j. This is necessary to reduce redundant information which can lead to overconfident estimations. In this case, the method employed for correction stage of the filter and to update the weights of hypotheses are GMC and TPU respectively.

The localization error using inter-node observations in the case of the synthetic dataset for 20 beacons goes from 0.63 meters to 0.49 meters, whereas in the case of real experiments the localization error goes from 0.54 meters to 0.49 meters. The cumulative localization error in Fig. 15 shows how the localization error throughout the whole experiment is reduced when inter-node range measurements are used. This reduction in the localization error is a direct consequence of the reduction in the mapping errors but also in the convergence time. It should be noted that, while a beacon does not converge, the corrections related with its observations are less precise due to the amount of hypotheses of the beacon.

On the other hand, in Fig. 16 can be seen how inter-node range measurements reduce the mapping error by more than 45% for simulation and more than 6% for real experimentation. The convergence time is also reduced with inter-node observations as shown in Fig. 16e and Fig. 16f in more than 55% in simulation and more than 60% in real experimentation. The X axis represents the time stamps of the experiment and the Y axis the number of beacons which have converged to a single hypotheses. The blue line corresponds to the convergence time using inter-node range measurements whereas the red line corresponds to the convergence time without using inter-node range measurements. This reduction of the convergence time is dependent on the frequency at which inter-node observations are integrated in the filter. Simulations performed at different inter-node observation periods have shown that higher frequencies leads to faster convergences but may reduce filter stability.

5. Conclusion

This paper has presented a Range-only SLAM approach applied to aerial robotics based on the integration of Gaussian Mixtures in a EKF with undelayed initialization. RO-SLAM poses significant technological challenges with respect to other SLAM schemes because of the rank-deficiency of range-only observations which leads landmarks position to a spherical shell uniform distribution.

The RO-SLAM algorithm proposed in this paper inherits the advantages of the reduced parameterization presented by authors in [27] and improves the correction stage of the EKF with a novel technique which only requires a single correction equation. This observation model not only improves the computational requirements of the correction stage but also reduces the convergence time of hypotheses. Furthermore, the paper presents an improved scheme to update the weights of hypotheses which is based on the same independence assumption between landmark parameters made in [27] but presents better robustness, processing times and convergence and accuracy. Finally, the additional integration of range-only observations between static range sensors reduces the convergence time of hypotheses and improves the precision of mapping and localization errors up to a 60%.

The paper also benchmarked the proposed 3D RO-SLAM approaches with other state-of-the-art algorithms:

1. three different parameterizations of landmark positions: Classical Cartesian parameterization [47], the extended spherical parameterization [26] and the proposed reduced spherical parameterizations.
2. three different observation models: one based on classical Federated Information Sharing (FIS) [1], an extended version of FIS previously presented in [27], and the novel GMC model proposed in this paper.
3. three different strategies to update the weights of hypotheses: classical strategy employed in [47, 26], an improved version previously presented in [27], and the robust strategy proposed in this paper.

As there are no open-access implementations for centralized EKF 3D RO-SLAM, the authors implemented the classical and proposed approaches to compare the performance and accuracy of the methods.

Future work will be focused on the use of other filtering schemes like unscented Kalman filter for linearization problems or Information filters for scalability improvements, in order to compare the advantages

and disadvantages of these filters. The authors are also working on multi-SLAM and active perception
approaches which takes advantage of the reduced parameterization and the efficient correction approach
presented in this paper. Finally, some recent methods for odometry estimation based on optical-flow with
UAVs [48] will be studied for the predictive stage of the filter.

Acknowledgment

References

[1] J. Sol, A. Monin, M. Devy, T. Lemaire, Undelayed initialization in bearing only SLAM, in: 2005 IEEE/RSJ International Conference on Intelligent Robots and Systems, 2005. (IROS 2005), 2005, pp. 2499–2504. doi:10.1109/IROS.2005.1545392.

[2] L. Jing, P. Yang, A Localization Algorithm for Mobile Robots in RFID System, in: 2007 International Conference on Wireless Communications, Networking and Mobile Computing, 2007, pp. 2109–2112. doi:10.1109/WICOM.2007.527.

[3] P. Yang, W. Wu, Efficient Particle Filter Localization Algorithm in Dense Passive RFID Tag Environment, IEEE Transactions on Industrial Electronics 61 (10) (2014) 5641–5651. doi:10.1109/TIE.2014.2301737.

[4] F. Fabresse, F. Caballero, I. Maza, A. Ollero, Localization and mapping for aerial manipulation based on range-only measurements and visual markers, in: Robotics and Automation (ICRA), 2014 IEEE International Conference on, IEEE, 2014, pp. 2100–2106.

[5] H. Wang, J. Wan, R. Liu, A novel ranging method based on RSSI, Energy Procedia 12 (2011) 230–235. doi:10.1016/j.egypro.2011.10.032.
URL http://www.sciencedirect.com/science/article/pii/S1876610211018583

[6] P. Bahl, V. Padmanabhan, RADAR: an in-building RF-based user location and tracking system, in: IEEE INFOCOM 2000. Nineteenth Annual Joint Conference of the IEEE Computer and Communications Societies. Proceedings, Vol. 2, 2000, pp. 775–784 vol.2. doi:10.1109/INFCOM.2000.832252.

[7] P. Corral, E. Pena, R. Garcia, V. Almenar, A. de C. Lima, Distance estimation system based on ZigBee, in: 11th IEEE International Conference on Computational Science and Engineering Workshops, 2008. CSEWORKSHOPS '08, IEEE, 2008, pp. 405–411. doi:10.1109/CSEW.2008.79.

[8] N. T. GmbH, Real time location systems (RTLS) (apr 2007).
URL http://www.nanotron.com/EN/pdf/WP_RTLS.pdf

[9] N. B. Priyantha, A. Chakraborty, H. Balakrishnan, The cricket location-support system, in: Proceedings of the 6th Annual International Conference on Mobile Computing and Networking, MobiCom '00, ACM, New York, NY, USA, 2000, p. 3243. doi:10.1145/345910.345917.
URL http://doi.acm.org/10.1145/345910.345917

[10] Guoyu Fu, Jin Zhang, Wenyuan Chen, Fengchao Peng, Pei Yang, Chunlin Chen, Precise localization of mobile robots via odometry and wireless sensor network, Int J Adv Robotic Sy 10. doi:10.5772/56217.

[11] Y. . Lpez, M. E. d. C. Gmez, J. L. lvarez, F. L.-H. Andrs, Evaluation of an RSS-based indoor location system, Sensors and Actuators A: Physical 167 (1) (2011) 110–116. doi:10.1016/j.sna.2011.02.037.
URL http://www.sciencedirect.com/science/article/pii/S0924424711000999

[12] D. Herrero, H. Martnez, Range-only fuzzy voronoi-enhanced localization of mobile robots in wireless sensor networks, Robotica FirstView (2011) 1–15. doi:10.1017/S0263574711001263.

[13] M. Gholami, N. Cai, R. Brennan, An artificial neural network approach to the problem of wireless sensors network localization, Robotics and Computer-Integrated Manufacturing 29 (1) (2013) 96–109. doi:10.1016/j.rcim.2012.07.006.
URL http://www.sciencedirect.com/science/article/pii/S0736584512000907

[14] A. Gasparri, F. Pascucci, An interlaced extended information filter for self-localization in sensor networks, IEEE Transactions on Mobile Computing 9 (10) (2010) 1491–1504. doi:10.1109/TMC.2010.122.

[15] J. Gonzlez, J. Blanco, C. Galindo, A. Ortiz-de Galisteo, J. Fernndez-Madrigal, F. Moreno, J. Martnez, Mobile robot localization based on ultra-wide-band ranging: A particle filter approach, Robotics and Autonomous Systems 57 (5) (2009) 496–507. doi:10.1016/j.robot.2008.10.022.
URL http://www.sciencedirect.com/science/article/pii/S0921889008001747

[16] S. Li, X. Wang, S. Zhao, J. Wang, L. Li, Local semidefinite programming-based node localization system for wireless sensor network applications, IEEE Systems Journal Early Access Online. doi:10.1109/JSYST.2013.2260625.

[17] B. Ingwer, P. J. F. Groenen, Modern Multidimensional Scaling - Theory and Applications, Springer, New York, NY, 1997.
URL http://www.springer.com/statistics/social+sciences+%26+law/book/978-0-387-25150-9

[18] A. Ahmad, S. Huang, J. Wang, G. Dissanayake, A new state vector and a map joining algorithm for range-only SLAM, in: 2012 12th International Conference on Control Automation Robotics Vision (ICARCV), 2012, pp. 1024–1029. doi:10.1109/ICARCV.2012.6485298.

[19] D. Moore, J. Leonard, D. Rus, S. Teller, Robust distributed network localization with noisy range measurements, in: Proceedings of the 2Nd International Conference on Embedded Networked Sensor Systems, SenSys '04, ACM, New York,

21

NY, USA, 2004, p. 5061. `doi:10.1145/1031495.1031502`.
URL `http://doi.acm.org/10.1145/1031495.1031502`

[20] J. Djugash, S. Singh, G. Kantor, W. Zhang, Range-only SLAM for robots operating cooperatively with sensor networks, in: Proceedings 2006 IEEE International Conference on Robotics and Automation, 2006. ICRA 2006, 2006, pp. 2078–2084. `doi:10.1109/ROBOT.2006.1642011`.

[21] F. Caballero, L. Merino, I. Maza, A. Ollero, A particle filtering method for wireless sensor network localization with an aerial robot beacon, in: IEEE International Conference on Robotics and Automation, 2008. ICRA 2008, 2008, pp. 596 –601. `doi:10.1109/ROBOT.2008.4543271`.

[22] F. Caballero, L. Merino, P. Gil, I. Maza, A. Ollero, A probabilistic framework for entire WSN localization using a mobile robot, Robotics and Autonomous Systems 56 (10) (2008) 798–806. `doi:10.1016/j.robot.2008.06.003`.
URL `http://www.sciencedirect.com/science/article/pii/S0921889008000869`

[23] L. Génevé, O. Kermorgant, E. Laroche, A Composite Beacon Initialization for EKF Range-Only SLAM, in: IEEE/RSJ Int. Conf. on Intelligent Robots and Systems, 2015.
URL `https://hal.inria.fr/hal-01219746/document`

[24] E. Olson, J. Leonard, S. Teller, Robust range-only beacon localization, in: In Proceedings of Autonomous Underwater Vehicles, 2004, p. 6675.

[25] J. Djugash, S. Singh, Motion-aided network SLAM with range, The International Journal of Robotics Research 31 (5) (2012) 603 – 625.
URL `https://www.ri.cmu.edu/pub_files/2012/4/2012-IJRR-NetworkSLAM.pdf`

[26] F. Caballero, L. Merino, A. Ollero, A general gaussian-mixture approach for range-only mapping using multiple hypotheses, in: IEEE International Conference on Robotics and Automation (ICRA), 2010, 2010, pp. 4404–4409.

[27] F. R. Fabresse, F. Caballero, I. Maza, A. Ollero, Undelayed 3d RO-SLAM based on gaussian-mixture and reduced spherical parametrization, in: 2013 IEEE/RSJ International Conference on Intelligent Robots and Systems (IROS), Tokyo Big Sight, Tokyo, Japan, 2013, pp. 1555–1561. `doi:10.1109/IROS.2013.6696556`.

[28] B. Boots, G. J. Gordon, A spectral learning approach to range-only SLAM, arXiv:1207.2491.
URL `http://arxiv.org/abs/1207.2491`

[29] J. R. Spletzer, A New Approach to Range-only SLAM for Wireless Sensor Networks, CiteSeer, 2003.

[30] S. Thrun, W. Burgard, D. Fox, Probabilistic Robotics, The MIT Press, 2005.

[31] Z. Kurt-Yavuz, S. Yavuz, A comparison of EKF, UKF, FastSLAM2.0, and UKF-based FastSLAM algorithms, in: 2012 IEEE 16th International Conference on Intelligent Engineering Systems (INES), 2012, pp. 37 –43. `doi:10.1109/INES.2012.6249866`.

[32] J. Li, L. Cheng, H. Wu, L. Xiong, D. Wang, An overview of the simultaneous localization and mapping on mobile robot, in: 2012 Proceedings of International Conference on Modelling, Identification Control (ICMIC), 2012, pp. 358 –364.

[33] P. Yang, Efficient particle filter algorithm for ultrasonic sensor-based 2d range-only simultaneous localisation and mapping application, IET Wireless Sensor Systems 2 (4) (2012) 394 –401. `doi:10.1049/iet-wss.2011.0129`.

[34] Z. M. Wang, D. H. Miao, Z. J. Du, Simultaneous localization and mapping for mobile robot based on an improved particle filter algorithm, in: International Conference on Mechatronics and Automation, 2009. ICMA 2009, 2009, pp. 1106 –1110. `doi:10.1109/ICMA.2009.5246103`.

[35] D. Hai, Y. Li, H. Zhang, X. Li, Simultaneous localization and mapping of robot in wireless sensor network, in: 2010 IEEE International Conference on Intelligent Computing and Intelligent Systems (ICIS), Vol. 3, 2010, pp. 173 –178. `doi:10.1109/ICICISYS.2010.5658491`.

[36] J.-L. Blanco, J. Gonzalez, J. Fernandez-Madrigal, A pure probabilistic approach to range-only SLAM, in: IEEE International Conference on Robotics and Automation, 2008. ICRA 2008, 2008, pp. 1436–1441. `doi:10.1109/ROBOT.2008.4543404`.

[37] J.-L. Blanco, J.-A. Fernandez-Madrigal, J. Gonzalez, Efficient probabilistic range-only SLAM, in: IEEE/RSJ International Conference on Intelligent Robots and Systems, 2008. IROS 2008, 2008, pp. 1017 –1022. `doi:10.1109/IROS.2008.4650650`.

[38] A. Torres-Gonzalez, J. R. Martinez-de Dios, A. Ollero, Accurate fast-mapping Range-Only SLAM for UAS applications, in: Unmanned Aircraft Systems (ICUAS), 2015 International Conference on, IEEE, 2015, pp. 543–550.
URL `http://ieeexplore.ieee.org/xpls/abs_all.jsp?arnumber=7152334`

[39] J. Castellanos, J. Neira, J. Tardos, Multisensor fusion for simultaneous localization and map building, IEEE Transactions on Robotics and Automation 17 (6) (2001) 908–914. `doi:10.1109/70.976024`.

[40] J. Djugash, S. Singh, A robust method of localization and mapping using only range, in: O. Khatib, V. Kumar, G. J. Pappas (Eds.), Experimental Robotics, no. 54 in Springer Tracts in Advanced Robotics, Springer Berlin Heidelberg, 2009, pp. 341–351.
URL `http://link.springer.com/chapter/10.1007/978-3-642-00196-3_40`

[41] S. Bouabdallah, R. Siegwart, Full control of a quadrotor, in: IEEE/RSJ International Conference on Intelligent Robots and Systems, 2007. IROS 2007, 2007, pp. 153–158. `doi:10.1109/IROS.2007.4399042`.

[42] J. Hershey, P. Olsen, Approximating the kullback leibler divergence between gaussian mixture models, in: IEEE International Conference on Acoustics, Speech and Signal Processing, 2007. ICASSP 2007, Vol. 4, 2007, pp. IV–317 –IV–320. `doi:10.1109/ICASSP.2007.366913`.

[43] A. Runnalls, Kullback-leibler approach to gaussian mixture reduction, IEEE Transactions on Aerospace and Electronic Systems 43 (3) (2007) 989 –999. `doi:10.1109/TAES.2007.4383588`.

[44] Nanotron Technologies GmbH, nanoPAN development kit.
URL `http://www.nanotron.com/EN/PR_ic_modules.php#08`

[45] F. J. Perez-Grau, F. R. Fabresse, F. Caballero, A. Viguria, A. Ollero, Long-term aerial robot localization based on visual

odometry and radio-based ranging, in: 2016 International Conference on Unmanned Aircraft Systems (ICUAS), 2016.

[46] F. R. Fabresse, F. Caballero, I. Maza, A. Ollero, Robust range-only SLAM for aerial vehicles, in: 2014 International Conference on Unmanned Aircraft Systems (ICUAS), 2014, pp. 750–755. `doi:10.1109/ICUAS.2014.6842320`.

[47] J.-L. Blanco, J. Gonzlez, J.-A. Fernndez-Madrigal, Optimal filtering for non-parametric observation models: Applications to localization and SLAM, The International Journal of Robotics Research 29 (14) (2010) 1726–1742. `doi:10.1177/0278364910364165`.
URL `http://ijr.sagepub.com/content/29/14/1726`

[48] V. Grabe, H. Bulthoff, P. Giordano, Robust optical-flow based self-motion estimation for a quadrotor UAV, in: 2012 IEEE/RSJ International Conference on Intelligent Robots and Systems (IROS), 2012, pp. 2153–2159. `doi:10.1109/IROS.2012.6386234`.
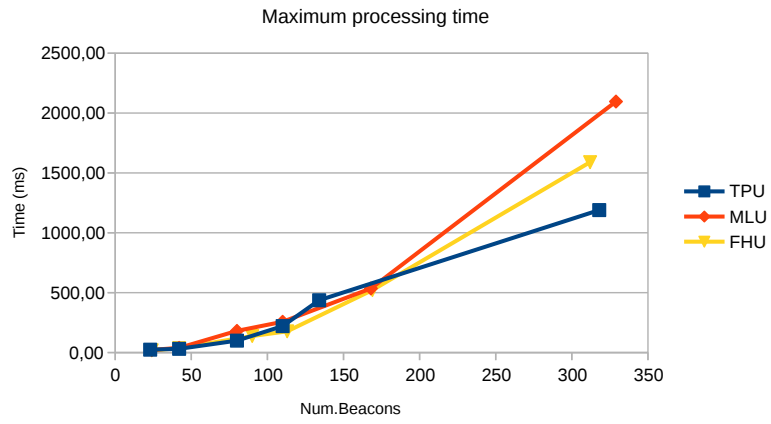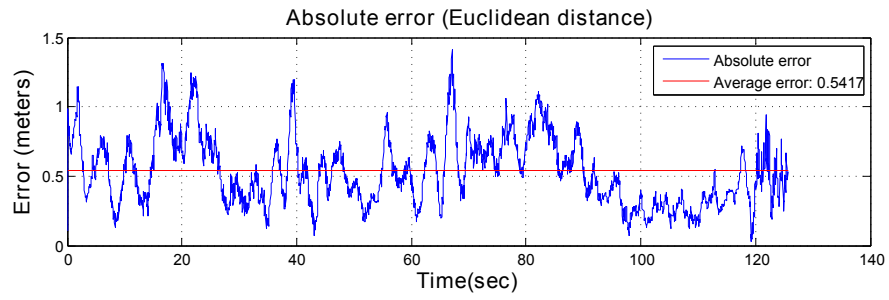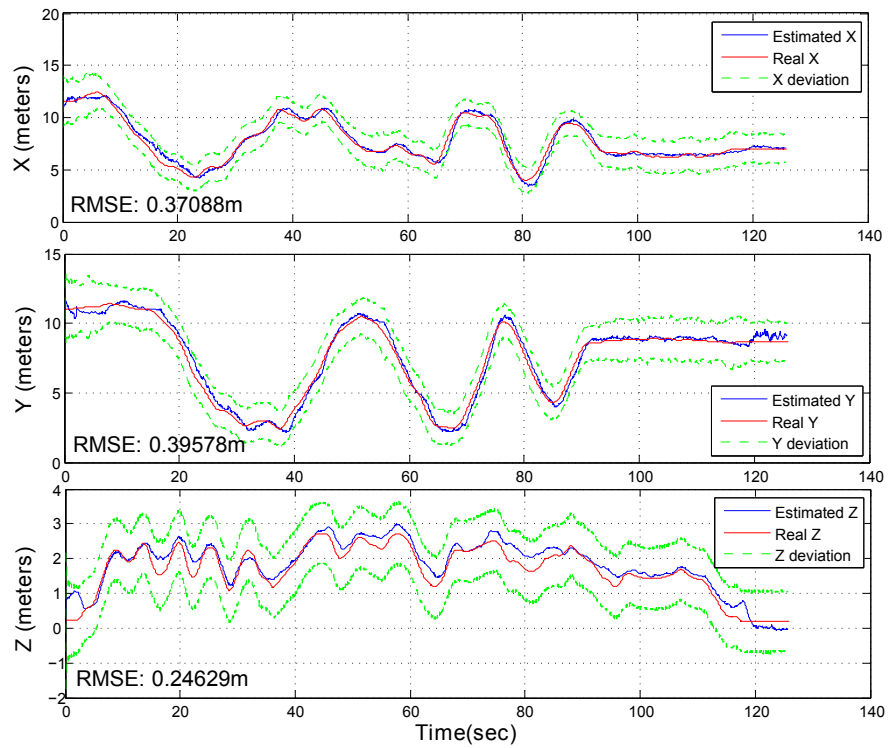
(a)
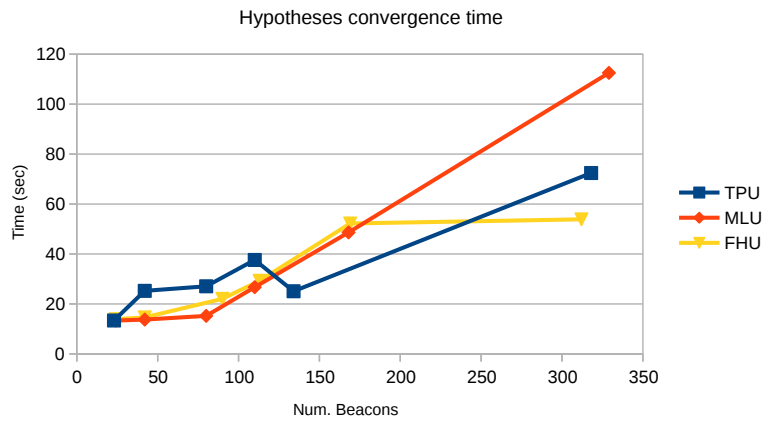
(b)
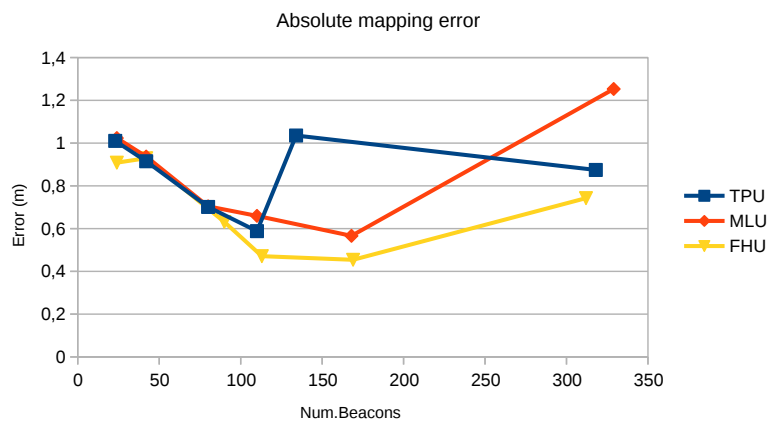
(c)

Figure 12: Comparison of (a) the processing time, (b) hypotheses convergence time and (c) averaged absolute mapping error for 10 beacons, different number of hypotheses and different weights update strategies.

Figure 13: Localization results for real dataset: (a) absolute localization error in blue and RMS error in red using GMC, (b) localization error with GMC along X, Y and Z axis. In (b) the blue continuous lines are estimates, the groundtruth is drawn with a red continuous line and the 3σ variance interval is drawn with a green dashed line. Localization errors are virtually the same for MHC.
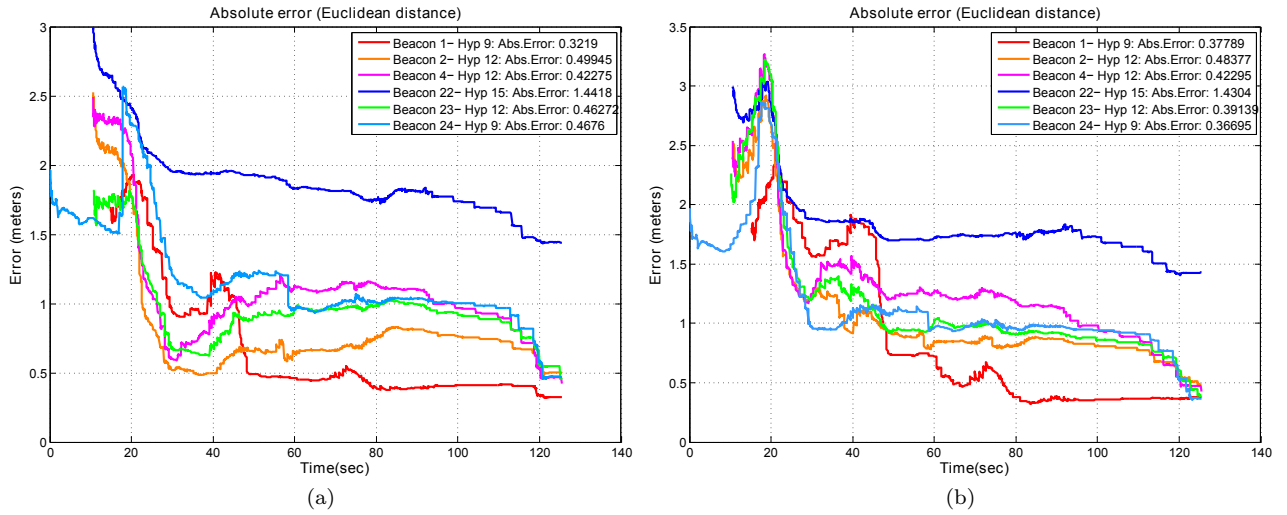
Figure 14: Mapping results for real dataset: (a) mapping results with MHC method and (b) mapping results with GMC method.
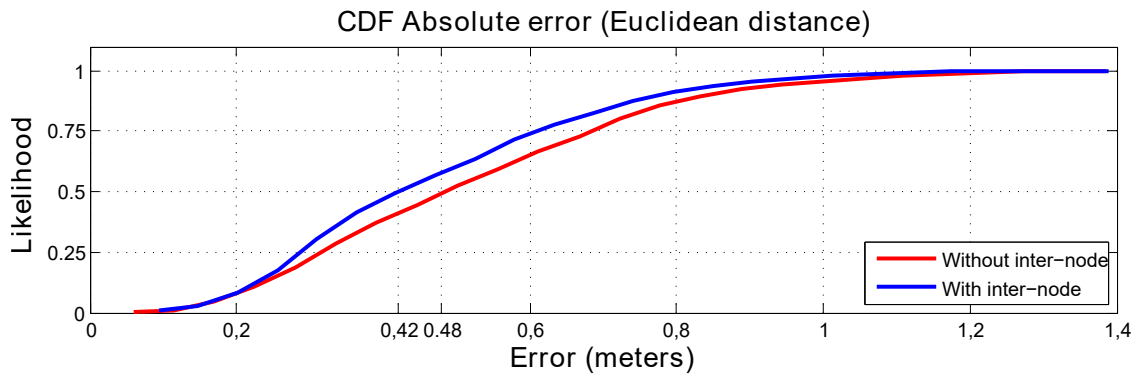

Figure 15: Cumulative distribution function of localization errors with (blue line) and without (blue line) inter-node range measurements for real dataset.
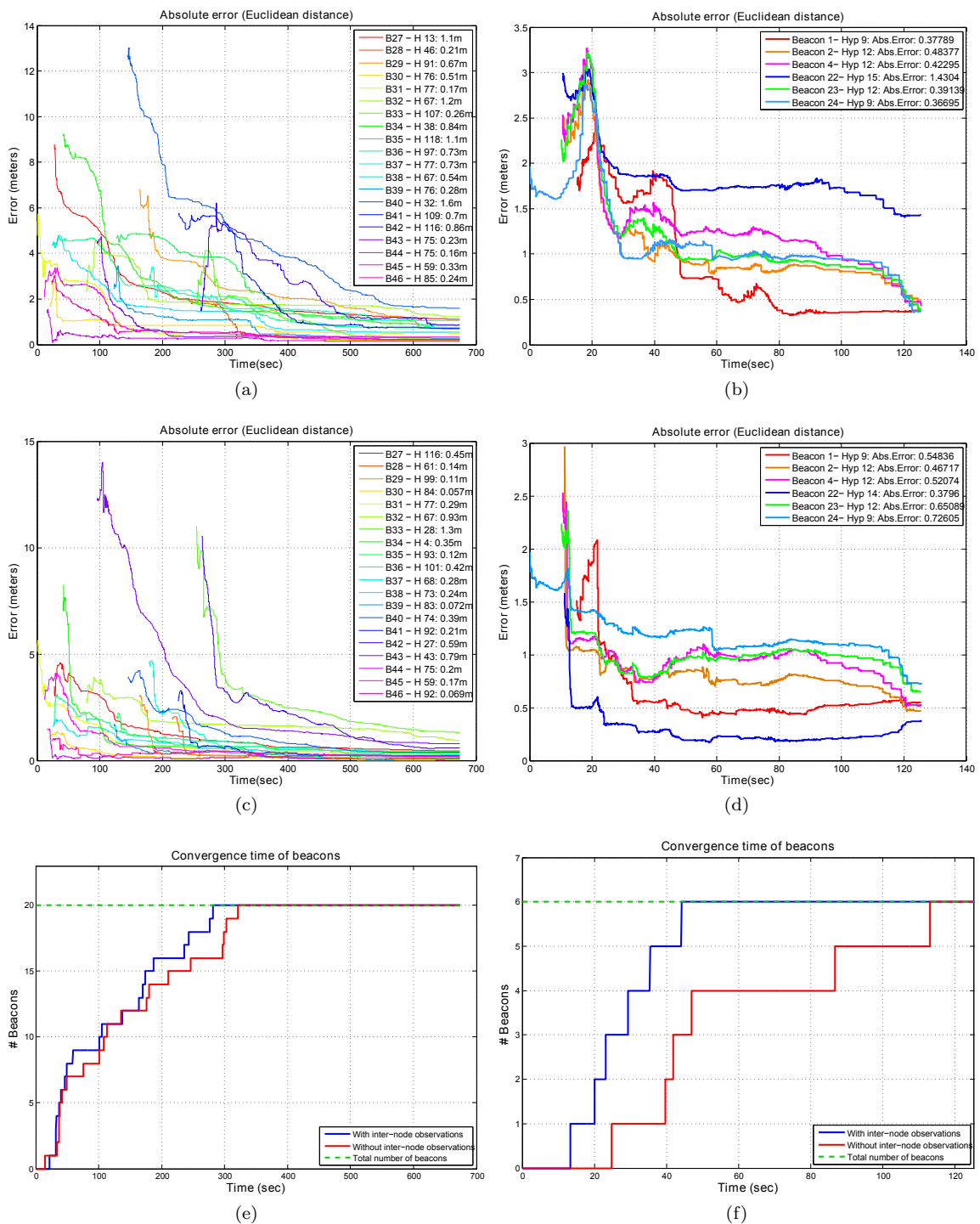
Figure 16: Experiments with inter-node range measurements: (a) simulation with 20 beacons and without inter-node observations, (b) real experiment without inter-node observations, (c) simulation with 20 beacons and inter-node observations, (d) real experiment with inter-node observations, (e) convergence time of beacons with (blue line) and without (red line) inter-node observations in synthetic dataset and (f) convergence time of beacons with (blue line) and without (red line) inter-node observations in real experimentation.